Article

Not peer-reviewed version

Assessment of Precipitation and Hydrological Droughts in South America through Statistically Downscaled CMIP6 Pro-jections

Glauber Willian de Souza Ferreira , Michelle Simões Reboita * , João Gabriel Martins Ribeiro , Christie André De Souza

Posted Date: 6 July 2023

doi: 10.20944/preprints202307.0373.v1

Keywords: Statistical downscaling; CMIP6; Precipitation; Drought; Climate change; South America

Article

Assessment of Precipitation and Hydrological Droughts in South America through Statistically Downscaled CMIP6 Projections

Glauber Willian de Souza Ferreira, Michelle Simões Reboita *, João Gabriel Martins Ribeiro, Christie André de Souza

Instituto de Recursos Naturais, Universidade Federal de Itajubá, Itajubá 37500-093, Brazil; glauber_ferreira@unifei.edu.br (G.W.d.S.F.); reboita@unifei.edu.br (M.S.R.); gabrielmr472@unifei.edu.br (J.G.M.R.); christie@unifei.edu.br (C.A.d.S.)

* Correspondence: reboita@unifei.edu.br

Abstract: Drought events are evident effects of climate change around the globe and yield several socio-economic impacts. Such effects are even more relevant for South America (SA) since different activities essential for the continent, like agriculture and energy generation, depend highly on water resources. Thus, this study aimed to evaluate future changes in precipitation and hydrological droughts occurrence in SA through climate projections from eight global climate models (GCMs) of CMIP6. To this end, statistical downscaling was applied to the projections with the Quantile Delta Mapping technique, and the method proved to be efficient in reducing systematic biases and preserving GCMs' trends. For the following decades, the results show considerable and statistically significant reductions in precipitation over most of SA, especially during the austral spring, with the most intense signal under the SSP5-8.5 forcing scenario. Furthermore, GCMs showed mixed signals about projections of the frequency and intensity of drought events. Still, they indicated agreement regarding the increase in duration and severity of events over all of SA and a substantial proportion of moderate and severe events over most of Brazil during the 21st century. These results can be helpful for better management of water resources by decision-makers and energy planners.

Keywords: statistical downscaling; CMIP6; precipitation; drought; climate change; South America

1. Introduction

Climate change is undeniable, as is its attribution to anthropogenic greenhouse gas-emitting activities, which have unequivocally intensified global warming, evidenced by the 1.1 °C increase in global surface temperature from 2011-2020 relative to 1850-1900 [1]. Additionally, best estimates indicate that continued greenhouse gas emissions will cause a 1.5 °C increase in the near term (2021-2040) [1]. Moreover, even if the countries fully implement the commitments made in the Paris Agreement, global warming is expected to exceed 2 °C by the end of the century [2,3]. The progressive warming will intensify the global hydrological cycle so that compound heatwaves and droughts are projected to become more frequent, including concurrent events in multiple locations [1].

Droughts are a natural phenomenon characterized by a continuous persistence of precipitation deficit, which occurs in almost all climate zones, including those with high precipitation rates, such as the Amazonia [4]. Prolonged periods of drought cause innumerable damages, such as losses in agriculture and livestock, contamination of waters, reduction of water availability for daily consumption and water energy generation, and environmental risks with fires [5,6]. Due to climate change and increasing temperatures, droughts are expected to increase in frequency and duration [7,8].

Studies with climate projections indicate an increased risk of extreme droughts in different parts of the world, depending on the seasons and drought indicators analyzed. For example, considering North America, studies with climate projections of phases 5 and 6 of the Coupled Model Intercomparison Project (CMIP) show an increase in the duration and frequency of droughts in the

southeast [9], central and northern [10–14] United States, and southwestern Canada [15]. Similarly, drought events are projected to intensify in parts of Asia [11–14,16,17], Africa [11,14,19], Europe [11,18], Oceania [11,13,14,18], and South America [11,13,14,18,20–25].

In South America (SA), climate change's effects on droughts are evident in different sectors, such as Northeastern and Southeastern Brazil, Amazonia, and the continent's southeast. The semi-arid Northeast of Brazil (NEB) is one of the historically most vulnerable regions to droughts [26], with several events recorded since the 16th century [26,27], and numerous socio-economic impacts such as damage to agricultural production, livestock, loss of human life from hunger, malnutrition, and disease, migrations to urban centers, and losses in regional and national economies [27]. The recent drought that began in 2012 and extended partially into 2018 (considered the most severe in recent decades) prompted public damage management policies that lessened the drought's impacts but were insufficient to contain its effects on nearly nine million people [22,27,28]. Towards the end of the 21st century, CMIP5 climate projections under the RCP-8.5 scenario indicate an increase of up to 54% in the proportion of areas under water stress conditions in the NEB, considering warming above 4 °C [27].

Southeastern Brazil (SEB) has also experienced some of the worst droughts in recent decades, such as in 2001 [29], 2014/2015 [30–34], 2018 [6], and most recently, in 2020/2021 [35]. Although in the 2014/2015 event, Brazil already had an interconnected electric system, which avoided an electric crisis in the country (unlike the 2001 event), this drought presented the largest rainfall deficit since 1960 in the metropolitan region of São Paulo (one of the most populated regions of Brazil), causing a water crisis with reservoirs at extremely low levels [31,32,36]. Considering the climatology of droughts in the region, observational data from 1901-2010 indicated for the western and central (eastern) sectors of the state of São Paulo a tendency of increase (reduction) of severe drought events [5].

Several drought events have also occurred in the Amazonia (AMZ), accentuating forest fires, affecting the region's biota, and signaling the risk of a tipping point [37–40]. Furthermore, future scenarios suggest reduced rainfall and intensified droughts in the forest [23,24,37,41,42], which may strengthen the process of savannization of the biome [37,38,43]. Additionally, in the last decade, other Brazilian regions have also experienced severe droughts, such as the 2019/2020 droughts in the Brazilian Pantanal and Midwest [44–46] and the 2012/2013 and 2019/2020 droughts in southern Brazil (SB) [47,48].

Another South American region affected by droughts is Southeastern South America (SESA), which covers northern Argentina, Paraguay, Uruguay, and SB. The 2008/2009 drought in the region was among the most severe in the last 50 years [49]. Analyses of precipitation and soil moisture anomalies from 1979-2018 have shown that droughts tend to last up to three months in the sector, resulting in significant losses in agricultural production [50]. Additionally, several studies have shown an increasing trend of warm days/nights [51–54] and the occurrence of dry spells [54,55] in the region in the last decades.

Droughts are a complex and multiform phenomenon [35], and different quantitative indicators allow their assessment [56]. The Standardized Precipitation Index (SPI), developed by McKee et al. [57], quantifies the rainfall deficit or excess on different time scales. SPI on time scales greater than six months is employed to identify and characterize hydrological droughts, which cause reduced soil moisture levels, river flows, groundwater recharge, and reservoir levels [56,58,59]. The SPI index proves advantageous because besides allowing the evaluation of drought impacts on different hydrological cycle components (using different time scales), it requires only rainfall data as input variables in the index computation [58]. However, as SPI does not account for the temperature component, its analysis disregards evapotranspiration processes, which play an essential role in the hydrological cycle [56,58]. Despite its limitations, several studies have employed the SPI-12 index (SPI index on a 12-month time scale) due to its simplicity of implementation to identify hydrological droughts in SA [6,56,58,60–67].

In this context of climate research, global climate models (GCMs) are a primary tool for investigating climate system elements [68]. A new generation of GCMs from CMIP has recently been available to the scientific community, comprising the sixth phase (CMIP6) of the project's experiment.

 doi:10.20944/preprints202307.0373.v1

The CMIP6-GCMs present aspects of improvement over previous generations, such as higher spatial resolution and better parameterization schemes of the physical and biogeochemical processes of the climate system [69]. In addition, CMIP6 models employ the Scenario Model Intercomparison Project (ScenarioMIP), which provides climate projections based on the latest greenhouse gas emission and land use scenarios, the Shared Socio-economic Pathways (SSPs) [70]. SSPs characterize a more realistic socio-economic development by considering different social, economic, technological, and political scenarios [71].

Despite their crucial role in climate research, GCMs have limitations due to their coarse spatial resolution, which restricts their use in analyzing regional-scale processes and impacts. In this framework, dynamical and statistical downscaling techniques address these limitations of global models. Dynamical downscaling employs regional climate models (RCMs) that use initial and boundary conditions provided by GCMs, while statistical downscaling determines relationships between large-scale atmospheric circulation factors and local climate [72]. Dynamical downscaling is helpful for the analysis of local-scale climate phenomena, but such a procedure requires high computational costs [73]. On the other hand, statistical downscaling requires less computational effort and avoids the propagation of systematic errors arising from GCMs [74].

Regarding SA, one observes a literature more focused on the dynamical approach of air temperature, precipitation, and wind [75–85]. However, recent studies have also applied the statistical method and demonstrated its competence in representing the spatial distribution and extreme events of temperature and precipitation [74,83,86–91]. Research with statistical downscaling of precipitation projections from CMIP6 to SA showed that the Quantile Delta Mapping (QDM) bias correction technique, developed by Cannon et al. [92], performed well in correcting the systematic errors in the different quantiles of the probability distributions of the GCMs raw simulations, evidencing its ability in reproducing seasonal variability and extreme properties [91]. With the QDM technique, it is possible to use data as reanalysis to interpolate the historical projections to the reference dataset's spatial resolution and, from transfer functions, apply the same correction to future projections. The QDM method proved to be advantageous since it preserves the model-projected relative changes and trends (i.e., if a model has a dry trend in a specific region, it will be kept after the spatial disaggregation and bias correction) and corrects the systematic biases in the quantiles of the modeled data with respect to the observations [92].

Given the background, this study aims to: (a) apply the QDM bias correction technique and statistical downscaling to historical simulations and climate projections of precipitation from a CMIP6 multi-model ensemble; (b) employ the bias-corrected estimates to present a set of precipitation projections at intermediate resolution (50 km) in SA; (c) employ the bias-corrected projections and the SPI-12 Index to identify the four types of hydrological drought events (mild, moderate, severe, and extreme), and their aspects (frequency, duration, severity, intensity, and peak) in eight subdomains of SA. There is still a shortage of studies analyzing hydrological droughts in SA with post-processed projections from the CMIP6-GCMs, and this study intends to fill such a gap. In addition, this research can assist decision-makers and energy planners in better future management of water resources on the continent.

2. Materials and Methods

2.1. Study Area

The study area comprises the SA continent (Figure 1), located at latitudes 12°N-55°S. Its extensive latitudinal coverage provides a climate heterogeneity of tropical, subtropical, and extratropical regions, as well as a diverse geography that includes particular areas such as the Andes Mountains, the Atacama Desert, the Amazon Rainforest, and the semi-arid Northeast of Brazil [93,94]. The South American Monsoon System (SAMS) primarily influences the central SA, with two well-defined seasons marked by the rainy season from November to March and the dry season from May to September [93–95]. On the other hand, the subtropical western portion of the continent concentrates its rainfall in the austral winter months due to the passage of cold fronts and cut-off

Preprints (www.preprints.org) | NOT PEER-REVIEWED | Posted: 6 July 2023 doi:10.20944/preprints202307.0373.v1

lows [93,94]. Still, the northern portion of SA does not have a well-defined dry season, being strongly influenced by the Intertropical Convergence Zone (ITCZ), with maximum rainfall in the austral autumn and early winter [96], and presenting one of the wettest places in the globe [97].

The rectangles illustrated in Figure 1 indicate the subdomains selected to analyze hydrological drought events on the continent. We considered subdomain 8 (Patagonia) because, in this region, the Andes have a lower height, while for the other parts of the Cordillera, we did not perform analysis due to the reference data also having uncertainties [98].

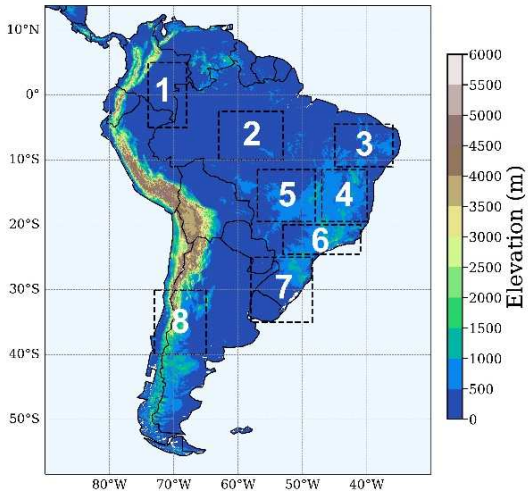

Figure 1. Illustration of the study area with elevation (m). Rectangles indicate subdomains selected for the analysis of drought events. Source: United States Geological Survey-Earth Resources Observation System (EROS) Center.

Table 2. Geographic coordinates of the subdomains selected for hydrological drought analysis.

Subdomain	Area
1	5°N–5°S 68°W–74°W
2	2.5°S–10°S 53°W–63°W
3	4.5°S–11°S 36°W–45°W
4	11.5°S–19.5°S 40°W–47°W
5	11.5°S–19.5°S 48°W–57°W
6	20°S–24.5°S 41°W–53°W
7	25°S–35°S 48.5°W–58°W
8	30°S–40°S 65°W–73°W

2.2 CMIP6-GCMs Selection

The study employed precipitation projections from eight CMIP6-GCMs, comprehending the historical period (1995-2014) and two greenhouse gas emission scenarios (SSP2-4.5 and SSP5-8.5) in the future period (2020-2099). The SSP2-4.5 scenario denotes a moderate emission scenario, while SSP5-8.5 considers a high greenhouse gas emission context, representing a period with little effort to mitigate climate change effects [70]. The GCMs dataset comprises precipitation projections every three hours provided on the Earth System Grid Federation (ESGF) platform (available at https://esgfnode.llnl.gov/search/cmip6).

At the early stage of this study (January 2022), we selected the models that best represented the South American climate in terms of precipitation and air temperature, which is a response to atmospheric circulation. To select the GCMs, we used the methodology of Rupp et al. [99], whereby

Preprints (www.preprints.org) | NOT PEER-REVIEWED | Posted: 6 July 2023 doi:10.20944/preprints202307.0373.v1

several metrics evaluate the best models based on regionally averaged properties and large-scale patterns. Thus, the identification of the best-performing models included the calculation of the following parameters with monthly data from 50 CMIP6-GCMs for different SA subdomains (figure not shown): (a) mean and standard deviation for each year (1995-2014); (b) spatial correlation calculated for each season (DJF, MAM, JJA, SON) and year (1995-2014) with Pearson's correlation coefficient; (c) mean amplitude, defined as the difference of the variables between January and July; (d) linear trend, calculated for complete time series (rather than by seasons) using the method of least squares and angular coefficients for the indication of a positive or negative trend.

Ranking the GCMs according to their performance is not trivial, as several statistical metrics and seasonal seasons are evaluated. Therefore, we compiled all the information by standardizing the metrics (giving equal weight/importance to each metric) to rank the GCMs in terms of performance according to the methodology proposed by Rupp et al. [99]. For each model i and metric j, the bias $E_{i,j}$ is calculated as:

$$E_{i,j} = \left|x_{obs,j} - x_{i,j}\right|, \quad (1)$$

where $E_{i,j}$ is the absolute error (absolute bias value), and $x_{obs,j}$ and $x_{i,j}$ are the observed and simulated metrics, respectively. The next step was to calculate the relative error $E^*_{i,j}$ (which can be interpreted as a standardized time series) by Equation 2:

$$E^*_{i,j} = \frac{E_{i,j} - \min(E_{i,j})}{\max(E_{i,j}) - \min(E_{i,j})}, \quad (2)$$

where $\max(E_{i,j})$ and $\min(E_{i,j})$ are the functions used to select a time series' maximum and minimum values, respectively. If the metric is a correlation, each function $\max(E_{i,j})$ or $\min(E_{i,j})$ is reversed. In this metric, since the absolute error $E_{i,j}$ is divided by the amplitude of the error, $E^*_{i,j} = 0$ indicates that the model has perfect performance and $E^*_{i,j} = 1$ denotes poor performance. According to Rupp et al. [99], the relative error is then summed over all statistical metrics m of a model, which provides the total relative error $E^*_{i,tot}$:

$$E^*_{i,tot} = \sum_{j=1}^{m} E^*_{i,j}, \quad (3) \quad (3)$$

The final step was to rank the models according to their relative error on a scale from 0 to 1, where each $E^*_{i,j}$ is divided by the maximum value of $E^*_{i,j}$. Figure 2 illustrates that the best models are on the left-hand side (values closest to zero). We could not necessarily select the best models shown in Figure 2 due to the absence of hourly/daily data and/or projections in the ESGF database. Thus, by concurrently analyzing the availability of high-frequency data and projections, the best models (indicated with red bars) were selected for this study (Table 2). Furthermore, three selected GCMs (EC-Earth3, IPSL-CM6A-LR, and MPI-ESM1-2-LR) were previously validated and performed well in representing the SA climate [100]. Although a good simulation of the historical period does not determine more accurate climate projections for the same model, it ensures more reliable future estimates since the poor ability to simulate historical climate is likely reflected in poorer future projections [101].

Preprints (www.preprints.org) | NOT PEER-REVIEWED | Posted: 6 July 2023 doi:10.20944/preprints202307.0373.v1

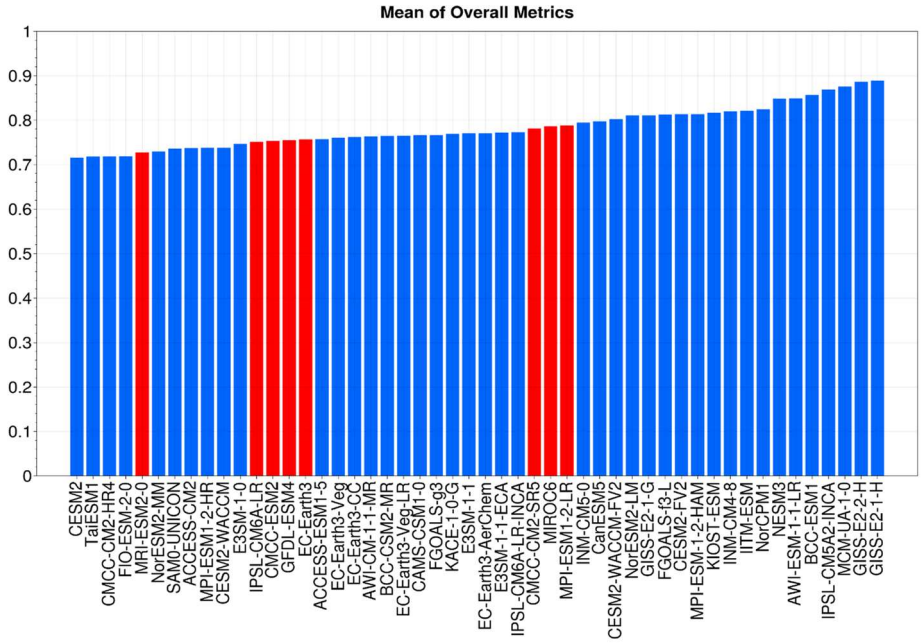

Figure 2. Ranking method based on Rupp et al. [99] obtained with monthly data from 50 CMIP6-GCMs for the historical period (1995-2014). Best performing models are located on the left side of the x-axis, and red bars indicate the models selected for the study.

Table 2. Information on each CMIP6-GCM employed in the study.

Model	Resolution (°Lat × °Lon)	Institute	Reference
CMCC-CM2-SR5	1.25 × 0.94	Fondazione Centro Euro-Mediterraneo sui Cambiamenti Climatici	Lovato and Peano [102]
CMCC-ESM2	1.25 × 0.94	Fondazione Centro Euro-Mediterraneo sui Cambiamenti Climatici	Lovato et al. [103]
EC-Earth3	0.70 × 0.70	EC-Earth Consortium	Döscher et al. [104]
GFDL-ESM4	1.25 × 1.00	Geophysical Fluid Dynamics Laboratory	Krasting et al. [105]
IPSL-CM6A-LR	2.50 × 1.26	Institut Pierre Simon Laplace	Boucher et al. [106]
MIROC6	1.41 × 1.41	Japan Agency for Marine-Earth Science and Technology	Tatebe and Watanabe [107]
MPI-ESM1-2-LR	0.94 × 0.94	Max Planck Institute for Meteorology	Wieners et al. [108]
MRI-ESM2-0	1.13 × 1.13	Meteorological Research Institute	Yukimoto et al. [109]

2.3 Reference Dataset

The study used precipitation analysis from the Climate Prediction Center Gauge-Based Analysis of Global Daily Precipitation (CPC) [110] to validate the historical simulations of the CMIP6-GCMs. For this, daily data from 1995 to 2014 were used, with 0.5° horizontal resolution (available at https://ftp.cpc.ncep.noaa.gov/precip/CPC_UNI_PRCP/GAUGE_GLB/RT/). CPC data proved adept

Preprints (www.preprints.org) | NOT PEER-REVIEWED | Posted: 6 July 2023 doi:10.20944/preprints202307.0373.v1

at representing average and seasonal precipitation patterns over most of SA [94] but present uncertainties in regions of complex topography such as the Andes Mountains [98].

We point out that the information in the CMIP6 tutorials does not clarify the period of daily precipitation accumulation. Precipitation data were obtained with a frequency of three hours, and the daily accumulation followed the recommendations of the World Meteorological Organization (WMO) [111] to avoid errors like comparing data with different periods for the daily accumulation. That is, the rainfall for a given day is accumulated from 1200 Z of the previous day to 1200 Z of the day in question. However, it is worth noting that the CMIP6 models provide the accumulations at 0130, 0430 Z until completing 24 hours. Thus, the accumulation was performed from 1330 Z to 1030 Z of the following day to be as close as possible to the WMO definition. Furthermore, CPC precipitation analysis also accumulates the daily rainfall in the 1200 to 1200 Z interval.

2.4. Bias Correction and Statistical Downscaling

One way to overcome the limitations imposed by the coarse resolution of GCMs is through statistical downscaling methods, which establish statistical relationships between model outputs and reference data [112]. Statistical downscaling techniques are classified into three types: transfer function or regression models, weather generators, and weather typing [110], and this study used transfer functions. This method was chosen due to its simplicity of implementation and for preserving time series trends (for more details, see Cannon et al. [92]). This methodology is also known as Bias Correction-Statistical Downscaling (BCSD).

This study used the BCSD method to downscale the simulations and projections of CMIP6-GCMs. Bias correction was performed with the QDM technique [92] to the historical simulations (1995-2014), and the transfer functions were applied to the future projections (2020-2099). According to Cannon et al. [92], the QDM technique preserves the model-projected trends and relative changes (e.g., if the GCM shows a dry trend in a given region, that trend will be maintained after bias correction) and corrects systematic biases in the quantiles of the modeled data relative to the reference one. Moreover, compared to the quantile mapping technique, the QDM technique proved advantageous because it is less susceptible to problems such as inflating relative trends in extreme values [92].

Before bias correction, spatial disaggregation was applied to the CMIP6-GCMs outputs, and the model data were downscaled to the 0.5° resolution as the CPC data with bilinear interpolation. Several studies show that bilinear interpolation provides consistent estimates by adjusting the spatially correlated behavior of the variable [91,113–120].

After spatial disaggregation, bias correction was applied with the QDM method. This method follows three steps [92]: first, the trend is removed from all projected individual quantiles. Next, the detrended quantiles are bias-corrected with the quantile mapping technique. Finally, the projected changes are superimposed on the bias-corrected outputs. Let o and p be the observed and projected data, and h and f are the historical and future periods, respectively. The definition of the non-exceedance probability of the observed ($x_{h,o}$) and projected ($x_{h,p}$) historical and future ($x_{f,p}$) data is accounted for as:

$$p_{f,p}(t) = F\left(x_{f,p}(t)\right)$$

$$p_{h,p}(t) = F\left(x_{h,p}(t)\right) \quad (4)$$

$$p_{h,o}(t) = F\left(x_{h,o}(t)\right)$$

where p and F denote the non-exceedance probability associated with a specific value in time and the cumulative distribution function (CDF), respectively. The change factor, which associates the historical simulation outputs with those of the future period, was calculated with Equation 5:

Preprints (www.preprints.org) | NOT PEER-REVIEWED | Posted: 6 July 2023 doi:10.20944/preprints202307.0373.v1

$$\Delta^{M}(t) = \frac{F_{f,p}^{-1}\left(p_{f,p}(t)\right)}{F_{h,p}^{-1}\left(p_{f,p}(t)\right)} = \frac{x_{f,p}(t)}{F_{h,p}^{-1}\left(p_{f,p}(t)\right)}, \quad (5)$$

where F^{-1} denotes the inverse CDF and $\Delta^{M}(t)$ is the multiplicative factor of change between the simulated quantiles of the historical and future periods. Finally, the bias correction in the future projections was obtained by applying the multiplicative relative change $\Delta^{M}(t)$ to the historical values with the corrected bias, according to Equation 6:

$$\hat{x}_{f,p}(t) = \Delta^{M}(t) \cdot F_{h,o}^{-1}\left(p_{f,p}(t)\right), \quad (6)$$

The historical period (1995-2014) was used for the training set to adjust the future projections (2020-2099) with the QDM algorithm. This time window was chosen due to computational resources and to follow the same reference period used by the International Panel on Climate Change (IPCC). The Python-based package *xclim* [121] was used to perform the calculations.

2.5 Test of Statistical Significance for the Difference in Climatological Mean Values

To assess whether the differences in mean climatological values in the future period (2020-2099) of the CMIP6-GCMs are statistically significant compared to the historical period (1995-2014), we used the Student's *t*-test. This test assumes the null hypothesis (H_0) of no difference between the two datasets against the alternative hypothesis of a difference between the two ensembles. The test was computed according to Equation 7:

$$t = \frac{\overline{X}_f - \overline{X}_h}{\sqrt{\frac{s_f^2}{n} + \frac{s_h^2}{n}}}, \quad (7)$$

where s_f and s_h are the standard deviation values of the future and historical datasets, respectively, and n comprises the number of values in each set. The associated degree of freedom v was estimated as:

$$v = \frac{\left(\frac{s_f^2}{n} + \frac{s_h^2}{n}\right)^2}{\frac{s_f^4}{n^2(n-1)} + \frac{s_h^4}{n^2(n-1)}}, \quad (8)$$

The test was performed using a significance level α of 5%. Thus, when the probability value (p-value) found was less than 5%, the null hypothesis of no difference between the two sets was rejected in favor of the alternative hypothesis, indicating statistical evidence of the difference between the mean values of the two periods evaluated.

2.6 Standardized Precipitation Index (SPI)

The SPI index, developed by McKee et al. [57], quantifies the rainfall deficit or excess on different time scales, evaluating the intensity of dry and wet periods. The SPI-12 index uses a time scale of 12 months. Besides identifying long-term rainfall patterns, SPI-12 can also be associated with flows, reservoir levels, and groundwater anomalies, helping to evaluate hydrological droughts [56,58].

According to Santos et al. [61], the first step in calculating the SPI is determining a probability density function that describes the time series. For this, the gamma function is a good fit for continuous variables with a lower limit equal to zero and no upper limit, widely used for studying historical precipitation series [61,122]. The gamma function is given by Equation 9:

$$g(x) = \frac{X^{\alpha-1} \cdot e^{\frac{-x}{\beta}}}{\beta^{\alpha}\Gamma(\alpha)}, \text{ para } X > 0, \quad (9)$$

Preprints (www.preprints.org) | NOT PEER-REVIEWED | Posted: 6 July 2023 doi:10.20944/preprints202307.0373.v1

where $\alpha > 0$ is the shape parameter, $\beta > 0$ is the scale parameter, $x > 0$ is the precipitation amount (mm) and $\Gamma(\alpha)$ is the full gamma function (for more details, see Wilks [122]). To estimate α and β parameters of the gamma distribution, equations 10 and 12 were used, respectively:

$$\alpha = \frac{1}{4A}\left(1 + \sqrt{1 + \frac{4A}{3}}\right), \quad (10)$$

$$A = \ln(\bar{x}) - \frac{\sum \ln(x)}{n}, \quad (11)$$

$$\beta = \frac{\bar{x}}{\alpha}, \quad (12)$$

where $\bar{x}$ is the mean rainfall, and n is the number of observations.

Thus, the cumulative distribution is then transformed into a normal probability distribution with a mean equal to zero and a standard deviation equal to one. Next, the cumulative probability of occurrence of each monthly value is estimated. This probability is applied to the inverse normal function to find the SPI value. The SPI is the difference of the observed rainfall minus the mean of the specific time interval, divided by the standard deviation, according to Equation 13:

$$SPI = Z_i = \frac{(P_i - \overline{P_i})}{\sigma_i}, \quad (13)$$

where P_i is the observed precipitation, $\overline{P_i}$ and σ_i are the mean and standard deviation of the fitted series, respectively.

As our results will show that the SSP5-8.5 scenario presents the most significant changes, the SPI-12 analysis was performed only under this scenario. Each bias-corrected CMIP6-GCM calculated SPI-12, and the BSCD ensemble (the bias-corrected CMIP6 ensemble) index was obtained by averaging the indices estimated by the individual models. Drought events were classified based on SPI values defined by McKee et al. [57]. Drought starts when the SPI falls below zero and ends when it becomes positive [57]. In this work, we used the thresholds defined by McKee et al. [57] (Table 3) to select and analyze all the drought events from mild to extreme categories. In addition, drought events were analyzed based on five characteristics: frequency (number of drought events in a period), duration (number of months between the first and last month of the event), severity (absolute sum of all SPI values during the event), intensity (ratio between severity and duration), and peak (largest absolute value of SPI recorded during the event).

Table 3. Drought events classification, adapted from McKee et al. [57].

SPI Values	Drought Category
0 to -0.99	Mild drought
-1.00 to -1.49	Moderate drought
-1.50 to -1.99	Severe drought
≤ -2.00	Extreme drought

3. Results and Discussion

3.1. Historical Simulations

The historical simulations (1995-2014) of precipitation obtained by the ensemble of eight CMIP6-GCMs before (raw ensemble) and after applying statistical downscaling (BCSD ensemble) are presented in Figure 3. Considering the austral summer (DJF), the raw ensemble tends to overestimate precipitation over most of Brazil and the west coast of SA (Figure 3a5). Contrarily, underestimates

 doi:10.20944/preprints202307.0373.v1

occur in northwest SA and north-central Argentina. In addition, the overestimation of rainfall over the Andes is notable. During summer, precipitation patterns exhibit a northwest-southeast orientation over the continent due to the action of the South Atlantic Convergence Zone (SACZ) [94]. On average, the raw ensemble represents the continental distribution of rainfall associated with the SACZ, but it amplifies and shifts the core of maximum precipitation to the southeast and northeast of SA.

The underestimation of precipitation during summer over northwestern SA and northern Brazil is also seen in other studies with CMIP6 models [123–125], as well as by CMIP5 models [126], associated with a less satisfactory representation of the Intertropical Convergence Zone (ITCZ), arising from the models' oversensitivity to sea surface temperature (SST) and deficiency in simulating surface wind convergence. Although the CMIP6 models show considerable improvement in reproducing rainfall magnitudes over SA relative to the CMIP5 models, the simulation of ITCZ position and intensity is still deficient, which partially justifies the negative rainfall biases over northern Brazil and northern SA [125]. The systematic underestimation of rainfall in the Amazon Basin is due to an insufficient representation of different processes such as cumulus convection, biosphere-atmosphere interactions in the forest, soil moisture, and surface processes, as well as a low coverage of rainfall stations in the region, which influences the analysis of the magnitude and location of precipitation [127].

In addition, GCMs tend to produce overly intense precipitation over the central Andes in Bolivia, Peru, Ecuador, and southwestern Colombia due to excessive modeled convection and lack of topographic representativeness. In addition, validating the simulations in these areas includes many uncertainties due to the scarcity of rainfall stations in mountainous regions [123,128]. Historical simulations of the CMIP6 ensemble without bias correction indicate better performance in reproducing precipitation patterns in SA during winter and spring, reiterating previous results [125].

Considering the BCSD ensemble, one notices a significant reduction of biases across the continent, especially on the west coast of SA and northeastern Brazil. Despite a better representation of the intensity and location of rainfall maxima associated with the SACZ, the ensemble still overestimates precipitation at the center of the continental SACZ, which is mainly controlled by internal climate variability and has low or negligible predictability associated with SST variations [129,130].

Preprints (www.preprints.org) | NOT PEER-REVIEWED | Posted: 6 July 2023 doi:10.20944/preprints202307.0373.v1

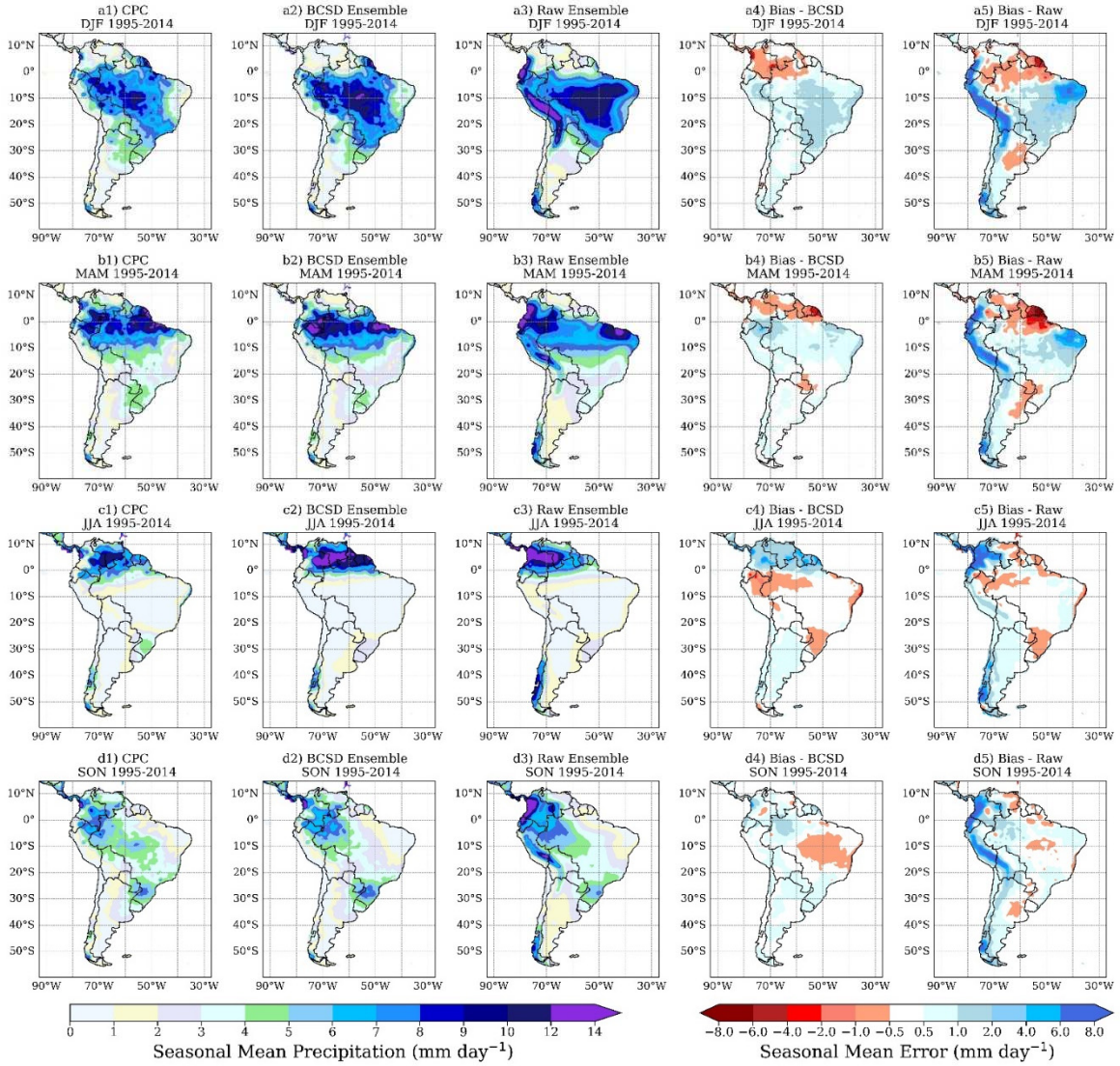

Figure 3. Seasonal climatology of precipitation (mm day^{-1}) in the historical period (1995-2014) obtained by CPC (first left column), BCSD ensemble (CMIP6 ensemble with BCSD) (second left column), raw ensemble (CMIP6 ensemble without BCSD) (middle column), and seasonal bias (mm day^{-1}) between the BCSD ensemble and CPC (second right column) and between the raw ensemble and CPC (first right column).

Similarly, during austral autumn (Figure 3b4), there is a marked reduction in the ensemble systematic biases, and the errors concentrate in northern SA, portions of north and northeastern Brazil, northeastern Peru, central Brazil, and western Chaco. Considering the rainfall biases north of 10°S obtained by the raw ensemble (Figure 3b3), BCSD adjusts the spatial distribution of rainfall, providing a simulated field analogous to the observed one, although with the persistence of larger overestimates in the far north of Peru and Brazil (Figure 3b2).

In the winter and spring seasons, the reducing raw ensemble's systematic errors in most of SA is notable, mainly on the continent's west coast and portions of Colombia and Venezuela (Figures 3c4 and 3d4). In winter, rainfall overestimates concentrate on the north of the equator, partially justified by the less satisfactory representation of the ITCZ by GCMs, while in spring, the positive precipitation bias in western Amazonas persists even after correction. In summary, we conclude that BCSD efficiently reduces the systematic errors of GCMs and ensures more reliable projections about future climate conditions. In general, the biases that persist after applying the correction occur in problematic sectors for global climate modeling, such as the tropical region and continental portion of the SACZ.

Preprints (www.preprints.org) | NOT PEER-REVIEWED | Posted: 6 July 2023 doi:10.20944/preprints202307.0373.v1

3.2. BCSD Ensemble Projections of Precipitation under the SSP2-4.5 and SSP5-8.5 Forcing Scenarios

Figures 4 and 5 present the precipitation climate projections obtained by the BCSD ensemble under the SSP2-4.5 and SSP5-8.5 forcing scenarios, respectively. Under the SSP2-4.5 scenario, BCSD ensemble projects for summer and fall increase by up to 10% over much of Brazil for the coming decades. From 2080, up to 20% growth is projected in Brazil's southeastern and northeastern sectors. In contrast, up to 20% reductions are projected in the extreme north of SA, with their sign diminished by the end of the 21st century.

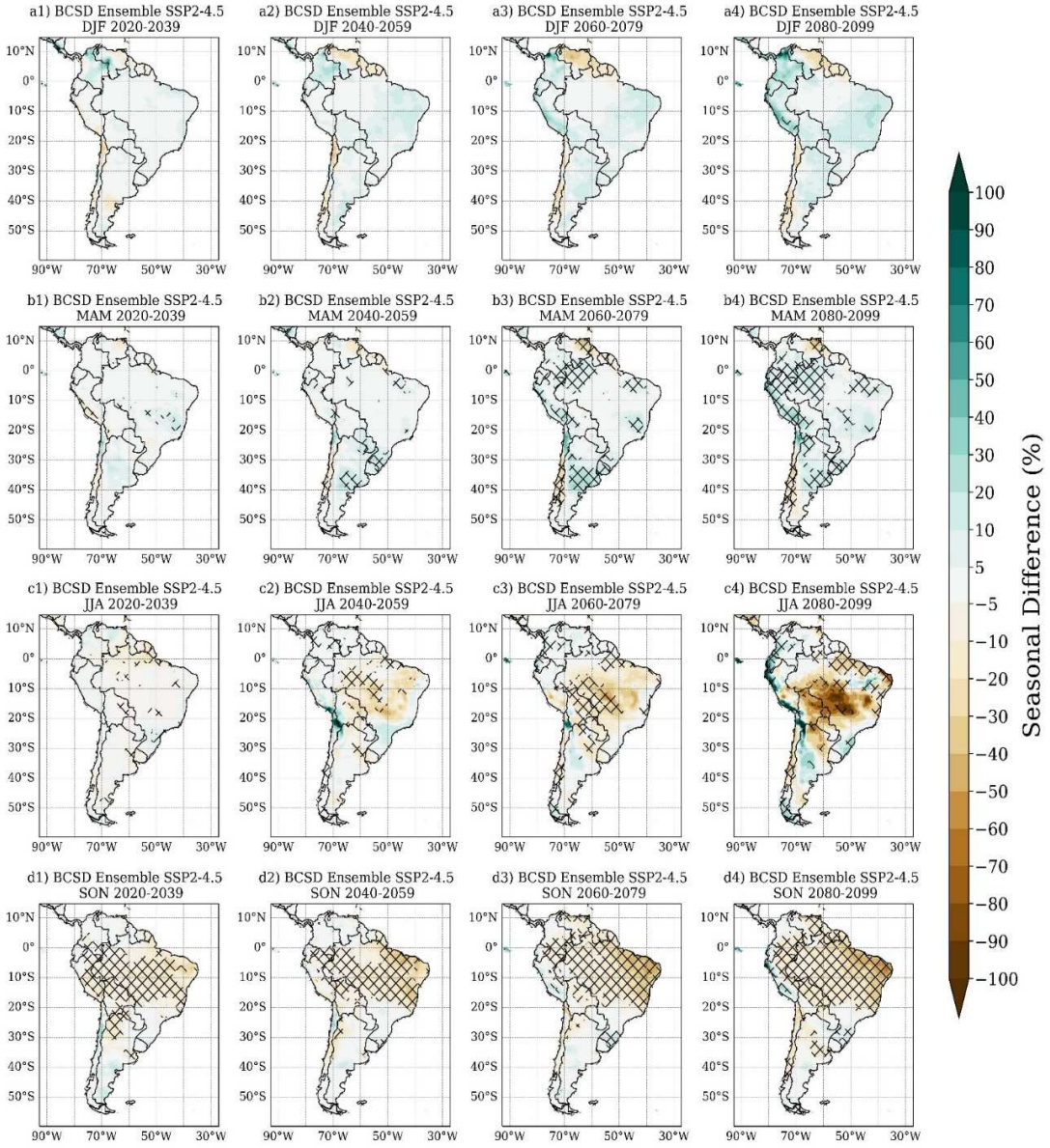

Figure 4. Seasonal differences of precipitation (%) between the future (2020-2039, 2040-2059, 2060-2079, 2080-2099) and historical period (1995-2014), projected by the BCSD ensemble under the SSP2-4.5 forcing scenario. Hatched areas indicate statistical significance at a 95% confidence level.

Preprints (www.preprints.org) | NOT PEER-REVIEWED | Posted: 6 July 2023 doi:10.20944/preprints202307.0373.v1

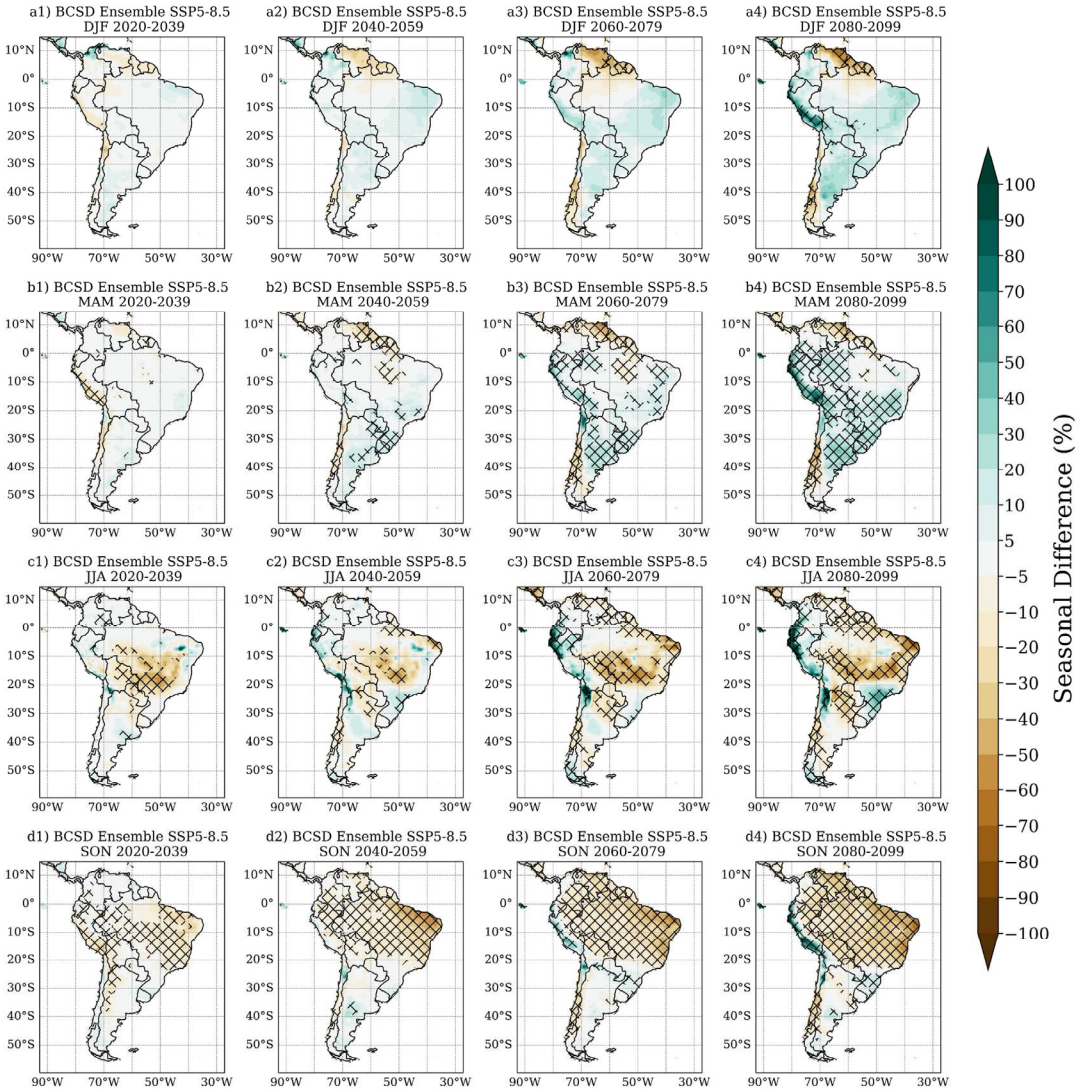

Figure 5. Seasonal differences of precipitation (%) between the future (2020-2039, 2040-2059, 2060-2079, 2080-2099) and historical period (1995-2014), projected by the BCSD ensemble under the SSP5-8.5 forcing scenario. Hatched areas indicate statistical significance at a 95% confidence level.

In the winter season (Figure 4c), the BCSD ensemble projects more expressive reductions starting in 2040, with regions of maximum decrease (up to 50%) beginning in 2080 in the central-western and northeastern Brazil sectors. In the spring (Figure 4d), the BCSD ensemble projects a significant reduction in rainfall, intensified after 2060, with reductions above 20% in large parts of central and northeastern Brazil. The results obtained here partially agree with those of other studies that used projections from the CMIP5 and CMIP6 models. Under the RCP4.5 forcing scenario, mean annual patterns from the ensemble of 26 CMIP5 models indicate decreases of up to 150 mm year-1 in the far north of SA, as well as decreases in annual rainfall over much of central SA, a slight increase over isolated portions of Northeast Brazil, and larger increases over southern Brazil [131].

Similarly, the CMIP5 ensemble indicates increased rainfall over southeastern SA and reduced rainfall over Amazonia and northern SA during the summer of 2050-2080 [23]. In winter, increased precipitation is also seen over western SA, extending from Ecuador to Argentina [23], a pattern analogous to that found here. Additionally, an ensemble composed of 38 CMIP6-GMCs projects increased precipitation (~0.3 mm day^{-1}) over Northeast and South Brazil sectors during the summer of 2040-2059 and a reduction of the same magnitude over nearly all of SA during the winter [123]. For the period 2080-2099, projections show even wetter (drier) conditions in southern Brazil (Amazonas and northern SA) during summer and intensified rainfall reduction across the continent

 doi:10.20944/preprints202307.0373.v1

during winter [123]. On the other hand, a study with the global HadGEM2-ES model nested with the Eta regional model under the RCP4.5 forcing scenario shows a projection of increased precipitation over most of the Amazon Basin, southern Brazil, and the northern portion of the coastal coast of Northeast Brazil, as well as decreased rainfall over much of the Midwest, Southeast, and central Northeast regions of Brazil [132]. We stress that the similarities and differences between the results of the studies are due to factors such as different models used, emission scenarios employed, reference periods chosen, and validation data.

Considering the SSP5-8.5 emission scenario (Figure 5), spatial patterns of projected seasonal change in precipitation are similar to those obtained for the SSP2-4.5 scenario but with the most intense sign of change. During summer (Figure 5a), an average increase of 10% is projected over most of Brazil and Argentina, and the growth intensifies after 2060, principally over portions of Northeastern Brazil and central-southern Argentina. The changes in fall (Figure 5b) are similar to the SSP2-4.5 scenario but indicate more intense precipitation increases in the Bahia state (Brazil), southern Brazil, central-eastern Argentina, and the central Andes.

In winter (Figure 5c), the BCSD ensemble projects rainfall decrease over much of central Brazil and Bolivia, extending into northern Argentina and southeastern, northeastern, and north Brazil. From 2060 onwards, the BCSD ensemble shows decreases of up to 50% in the Midwest and coastal Northeast areas. In contrast, a substantial rainfall increase for Brazil's southeast and south coasts is observed from 2080 onward. In spring (Figure 5d), the projections indicate more drastic changes, with decreases of more than 10% over most of Brazil and northern SA, with more intense reductions (up to 50%) over the northern portion of coastal Northeast Brazil. During this season, projected increases in precipitation occur in isolated regions such as the coasts of Peru and Ecuador and northern Chile.

The results agree with those of Ruffato-Ferreira et al. [132], in which there is a trend of increasing water scarcity mainly in central Brazil, as well as a progressive increase in water availability in the southern and southeastern Atlantic basins, favoring southern Brazil. In addition, the São Francisco River Basin is the most vulnerable in a maximum emission scenario, accentuating water scarcity in Northeast Brazil. Similarly, CMIP5 projections indicate increases of about 100 mm year^{-1} by the end of the 21st century in southern Brazil and parts of Peru, Ecuador, Colombia, and Venezuela. In comparison, areas between south Chile and Argentina and the far north of SA may experience reductions of up to 150 mm year^{-1} [131].

The higher severity of precipitation reductions in SA under the SSP5-8.5 scenario was also obtained by CMIP5 models nested with different regional climate models [23,24,133]. Among the possible causes for the dry conditions projected for Amazonia and northern SA is the weakening of the northeast trade winds at the end of the 21st century, inducing a decrease in moisture transport from the ocean to the continent [23,73]. Additionally, studies with CMIP6-GCMs under the SSP5-8.5 forcing scenario also provide projections of expressive precipitation reduction over much of the continent, mainly in the Midwest, Southeast, Northeast, and North of Brazil and northern SA, with decreases of up to 1.2 mm day^{-1} in the most affected regions [123,125]. On the other hand, SESA and southern Brazil will likely experience higher rainfall volumes in the coming decades, exposing these regions to the progressive frequency of extreme daily precipitation events and an increase in the number of consecutive wet days [23].

Analyses of projected changes in rainfall with GCMs from CMIP3, CMIP5, and CMIP6 over Brazil show that the projected signal depends on the CMIP generation considered, except for southern Brazil, where an increase is seen in all cases [134]. While CMIP3 projects an increase in rainfall in northern Brazil (especially in the western portion), CMIP5 and CMIP6 models project a reduction. In Northeast Brazil, the projections are also divergent among the CMIP generations, with CMIP5 indicating an increase in rainfall throughout the territory. At the same time, CMIP3 and CMIP6 project an increase (reduction) in rainfall in the region's northern (southern) sector. In the Midwest and Southeast regions, the sign depends on the family of CMIP used, with increased precipitation projected by CMIP5 and decreased rainfall estimated by CMIP3 and CMIP6. In summary, multi-model ensembles show that CMIP3 most accurately represents precipitation

Preprints (www.preprints.org) | NOT PEER-REVIEWED | Posted: 6 July 2023 doi:10.20944/preprints202307.0373.v1

extremes in Northeastern Brazil, while CMIP5 performs best for the Midwest, and CMIP6 provides the most accurate projections for the remaining Brazilian regions [134].

Finally, we recommend caution for energy planning with the projections analyzed here. More robust evaluations should consider the vegetation of different biomes since it plays a crucial role in the water balance and greater detail of the projected scenarios of land use and land cover changes. Furthermore, intrinsic to the process of climate modeling, the uncertainties and inaccuracies associated with different models limit a greater assertiveness and require pondering in decision-making based on the projections.

3.3. Temporal Series of the BCSD Ensemble SPI-12 Index under the SSP5-8.5 Forcing Scenario

Figure 6 shows the SPI-12 temporal series (2020-2099) provided by the BCSD ensemble under the SSP5-8.5 emission scenario for eight SA subdomains. The SPI-12 index was obtained by averaging the indices calculated for each individual projection. In R1 (northwestern Amazonia), 31 drought episodes were identified between 2020-2099, all belonging to the mild drought category. The longest episode occurs from 07/2086 to 09/2088, totaling 37 months, followed by the episode from 06/2065 to 05/2068 (36 months) and severity of 10.02. In addition, other long-lasting drought episodes occur from 11/2044 to 08/2047 and from 08/2049 to 05/2052 (34 months each).

For R2 (central Amazonia), 30 drought episodes were identified in the period 2020-2099, categorized as mild droughts, and 56% of the episodes (17 cases) have a duration of 10 months or longer. The longest episode occurs from 03/2061 to 11/2065 (57 months), with a severity of 13.89. Other longer episodes occur from 12/2085 to 02/2089 (39 months), from 04/2039 to 08/2041 (29 months), and from 10/2073 to 12/2075 (27 months).

Although different droughts have occurred in Amazonia during El Niño-Southern Oscillation (ENSO) events, SST anomalies in the tropical North Atlantic (TNA) also play an important role in the region's rainfall regime [4,37,40,135,136]. The anomalous warming in TNA is associated with the northward displacement of the ITCZ, changes in the north-south divergent circulation, and weakening of the trade winds and moisture flux from the tropical Atlantic, inducing a reduction of rainfall in the southern, northern, and eastern sectors of Amazonia [4,37,136]. Furthermore, ENSO events are related to anomalies in the east-west Walker circulation, with convection over the central Pacific and subsidence over east and central Amazonia [4,135,136].

In general, drought events related to warm SST anomalies in TNA show a north-south gradient with drier (wetter) conditions in southern (northern) Amazonia, while droughts linked to ENSO events show a southwest-northeast gradient with drier conditions in northeastern Amazonia [136]. However, overlapping effects of both teleconnection mechanisms also affect the region, such as the 2010 drought associated with successive ENSO episodes during the austral summer and the warmer TNA during the austral autumn and winter [37]. Similarly, the severe drought of 2015-2016 was associated with intense warm anomalies in the central Pacific and TNA, with marked effects in northeastern Amazonia [137].

Considering the occurrence of drought events in 2015-2100 relative to the 1850-2014 period under the SSP5-8.5 scenario, Wang et al. [14] found an increase in the frequency of droughts in northern SA during the 21st century, as well as more prolonged droughts and more than 50% increase in the extent of areas affected. On the other hand, the variability of drought-related statistical results provided by CMIP6 models is greater in the tropics than in other latitudinal zones, implying that GCMs need improvement in capturing drought-causing patterns in equatorial regions [7]. Furthermore, models from CMIP5 and CMIP6 indicate divergence in rainfall projections over the area, and models from CMIP6 show no improvement in simulating total precipitation and consecutive dry days relative to the previous generation of CMIP [138].

Preprints (www.preprints.org) | NOT PEER-REVIEWED | Posted: 6 July 2023 doi:10.20944/preprints202307.0373.v1

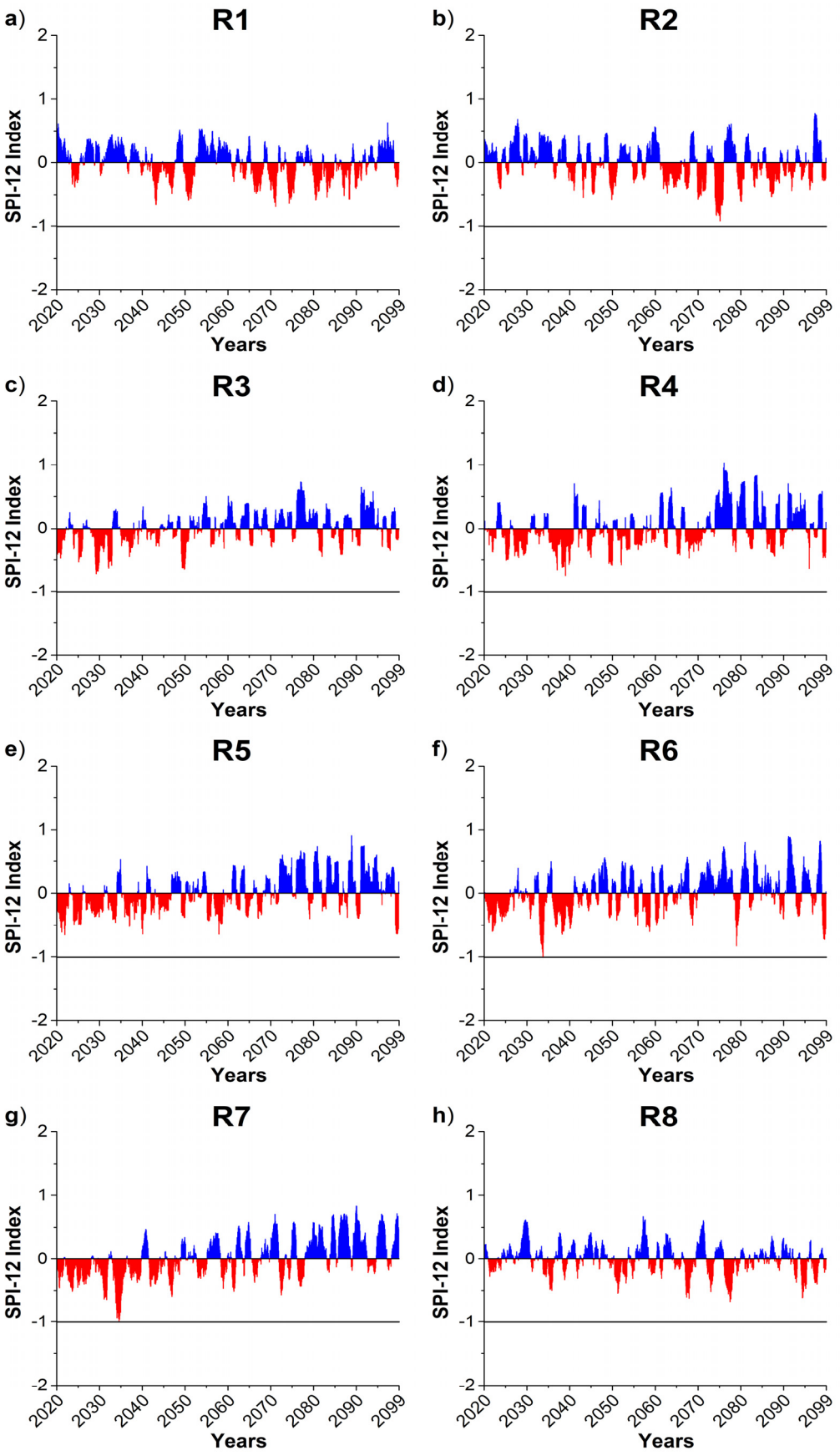

Figure 6. Temporal series (2020-2099) of the SPI-12 Index projected by the BCSD ensemble under the SSP5-8.5 scenario for eight SA subdomains. The black dashed line indicates the threshold for moderate droughts.

Preprints (www.preprints.org) | NOT PEER-REVIEWED | Posted: 6 July 2023 doi:10.20944/preprints202307.0373.v1

In R3 (northern sector of Northeast Brazil), 31 drought episodes were identified in 2020-2099, all belonging to the mild drought category. About 61% of the episodes (19 events) present a duration equal to or longer than 10 months. The longest-lasting hydrological drought episode occurs from 11/2027 to 12/2032 (62 months), followed by the episodes from 01/2041 to 02/2044 (38 months) and 12/2034 to 12/2037 (37 months). In R4 (central sector of Northeast Brazil), 32 hydrological drought episodes were counted in 2020-2099, all classified as mild droughts. About 72% of the episodes (23 cases) are 10 months or longer. Four longer-lasting episodes were obtained from 01/2035 to 12/2040 (72 months), from 11/2026 to 11/2030 (49 months), from 01/2067 to 12/2069 (36 months), and from 12/2085 to 02/2088 (27 months). Our results corroborate previous analyses since CMIP6 projections suggest an increase in the number of dry days in Northeast Brazil (mainly in DJF and MAM), with an estimated increase of up to 8.0 and 14.7% in the near (2016-2040) and far (2076-2100) futures, respectively, under the SSP5-8.5 scenario [139].

Precipitation in Northeast Brazil is marked by interannual variability and drought events are attributed to ENSO and the anomalously northern position of the ITCZ, resulting from a warmer TNA [12,37,136,140]. However, extratropical variability modes also influence rainfall distribution in the region, as analyses from 1980-2009 concluded that drought events in this period showed annular patterns in both hemispheres (South Annular Mode and North Annular Mode) well configured during DJF (pre-rainy season in the region), both in years with and without ENSO [141].

For R5 (Midwest region of Brazil), 31 drought episodes were identified, all classified as mild droughts, with the most extended episode from 11/2026 to 02/2031 (52 months), followed by other long-lasting events from 02/2043 to 10/2046 (45 months), and from 10/20635 to 11/2038 (38 months). About 61% of the drought episodes (19 cases) are 10 months or longer.

Marengo et al. [46] report no evident direct relationship between drought events in the region and SST anomalies in the Pacific and Atlantic oceans. While the 2019-2020 drought was associated with anomalous warming in TNA, earlier events occurred with simultaneous warming of the northern tropical and equatorial Pacific and cooling of TNA. Overall, the authors conclude that droughts in the region may be triggered by warmer SSTs in the North Atlantic and North Pacific (which promote the northward displacement of the ITCZ and reduce precipitation in southern Amazonia and the Midwest), which reduce moisture transport from Amazonia to the region. However, regional factors such as water balance and soil moisture influence the sector's interannual seasonality of droughts and floods. In this context, there is an increasing tendency in the water deficit in deforested regions due to the expansion of agriculture and cattle ranching, contributing to local warming and reduced precipitation [35].

In R6 (Southeast region of Brazil), 33 drought episodes were counted in the period 2020-2099, all belonging to the mild drought category, with the longest-lasting episode from 04/2020 to 01/2026 (70 months), followed by episodes with 61 months (from 12/2035 to 12/2040) and 23 months (11/2032 to 09/2034). Approximately 60% of projected drought episodes are 10 months or longer.

Analyses of SPI-1 and SPI-12 in the north and northwest areas of the Rio de Janeiro state for the 1967-2013 period indicated a higher occurrence of events in the moderately and extremely dry categories, as well as a higher frequency of droughts in the two regions of the state during ENSO cycles in both phases of the Pacific Decadal Oscillation [62]. Moreover, analyses of drought events in the Paraná River basin showed that hydrological droughts in the 1981-2021 period were the most severe and intense [35]. Furthermore, studies show that the severe drought of 2014-2015 was associated with anomalous warming in the western tropical Pacific that initiated a wave train along the south Pacific, which in turn resulted in anomalous anticyclonic circulation in the southwest Atlantic, expanding the west flank of the South Atlantic Subtropical Anticyclone (SASA) and restricting the entry of low-pressure systems into southeastern Brazil [30,32]. Additionally, analyses of summer droughts during 1961-2010 in the São Paulo state show a prevalence of anomalous subsidence of the Hadley cell's descending branch over the region, inhibiting convective activity in the sector [33].

In R7 (Southern Brazil and Uruguay region), 29 drought episodes were computed, all categorized as mild droughts, of which 62% (18 episodes) have a duration of 10 months or longer.

Preprints (www.preprints.org) | NOT PEER-REVIEWED | Posted: 6 July 2023 doi:10.20944/preprints202307.0373.v1

The longest drought episode refers to the period from 01/2022 to 01/2028 (73 months), followed by cases of 41 months (12/2032 to 04/2036) and 39 months (08/2036 to 10/2039). Many of the droughts that have occurred in the region are linked to the cold phase of ENSO (La Niña), but other factors also contribute to the onset and intensification of droughts in the sector, such as the development of atmospheric blockings in the south Pacific, warmer SST anomalies in TNA occurring concurrently with La Niña, as well as more regional and local aspects such as reduced moisture transport to the region caused by deforestation in Amazonia [49,50,142,143]. Attribution study infers that the rainfall deficit occurring in the Southern part of Brazil, Argentina, and Uruguay since 2019 is not only partially induced by the action of La Niña but also caused by higher temperatures that reduce water availability in the region, indicating that although the decrease in rainfall is associated with natural climate variability, the consequences of drought are becoming more severe due to increasing temperatures [143].

Finally, in R8 (western Patagonia), 40 drought episodes were identified in 2020-2099, all classified as mild droughts, of which 52.5% (21 cases) have a duration of 10 months or more. The longest-lasting episode occurs from 06/2050 to 07/2053 (38 months), followed by episodes of 32 months (01/2076 to 08/2078) and 28 months (09/2066 to 12/2068). This sector has experienced intense droughts recently [144], substantially affecting socio-economic activities in the region.

In conclusion, the BCSD ensemble shows that all SA subdomains analyzed are prone to drought episodes during the 21st century. Although the ensemble projects predominantly mild droughts, perhaps due to smoothing the most extreme projections, a considerable proportion of episodes last longer than 10 months. The significant occurrence of longer hydrological drought episodes corroborates analyses previously performed with CMIP6 models that indicated an increase in event duration during the 21st century under the SSP5-8.5 scenario in SA and a higher frequency of longer-lasting events [14].

3.4. Projections of Drought Parameters by the Bias-Corrected CMIP6-GCMs and BCSD Ensemble

Figures 7 and 8 show the droughts parameters projected by the eight bias-corrected CMIP6-GCMs, as well as by CPC (for the historical period only) and BCSD ensemble under the SSP5-8.5 scenario.

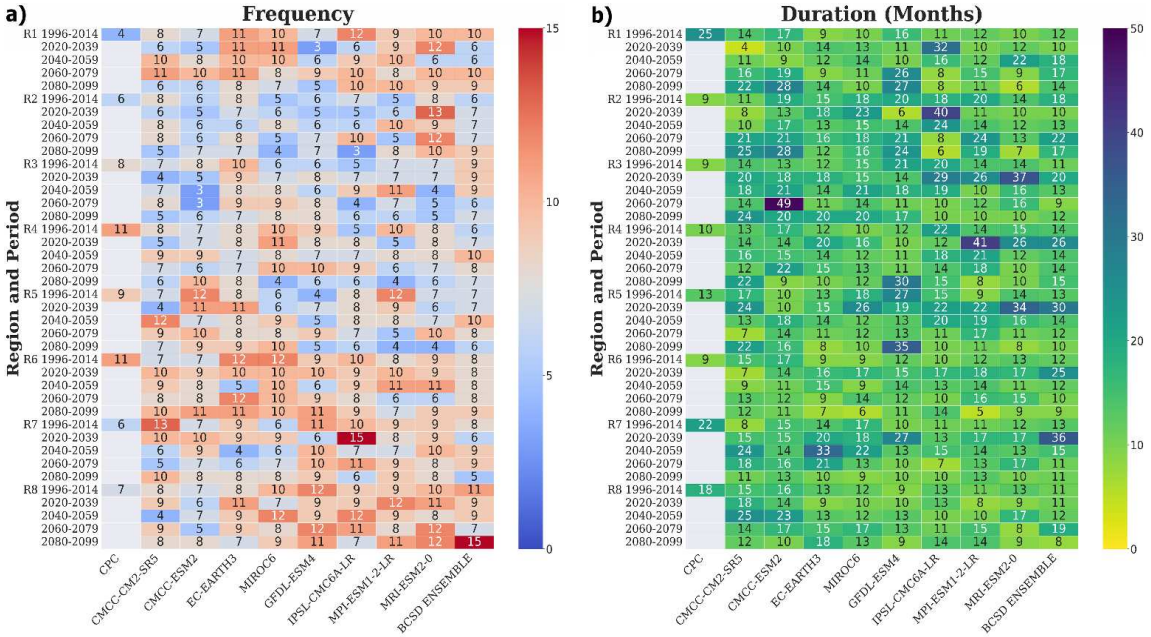

Figure 7. Heatmaps of drought frequency (a) and duration (b) projected by the bias-corrected CMIP6-GCMs and BCSD ensemble under the SSP5-8.5 scenario for eight subdomains of SA.

Preprints (www.preprints.org) | NOT PEER-REVIEWED | Posted: 6 July 2023 doi:10.20944/preprints202307.0373.v1

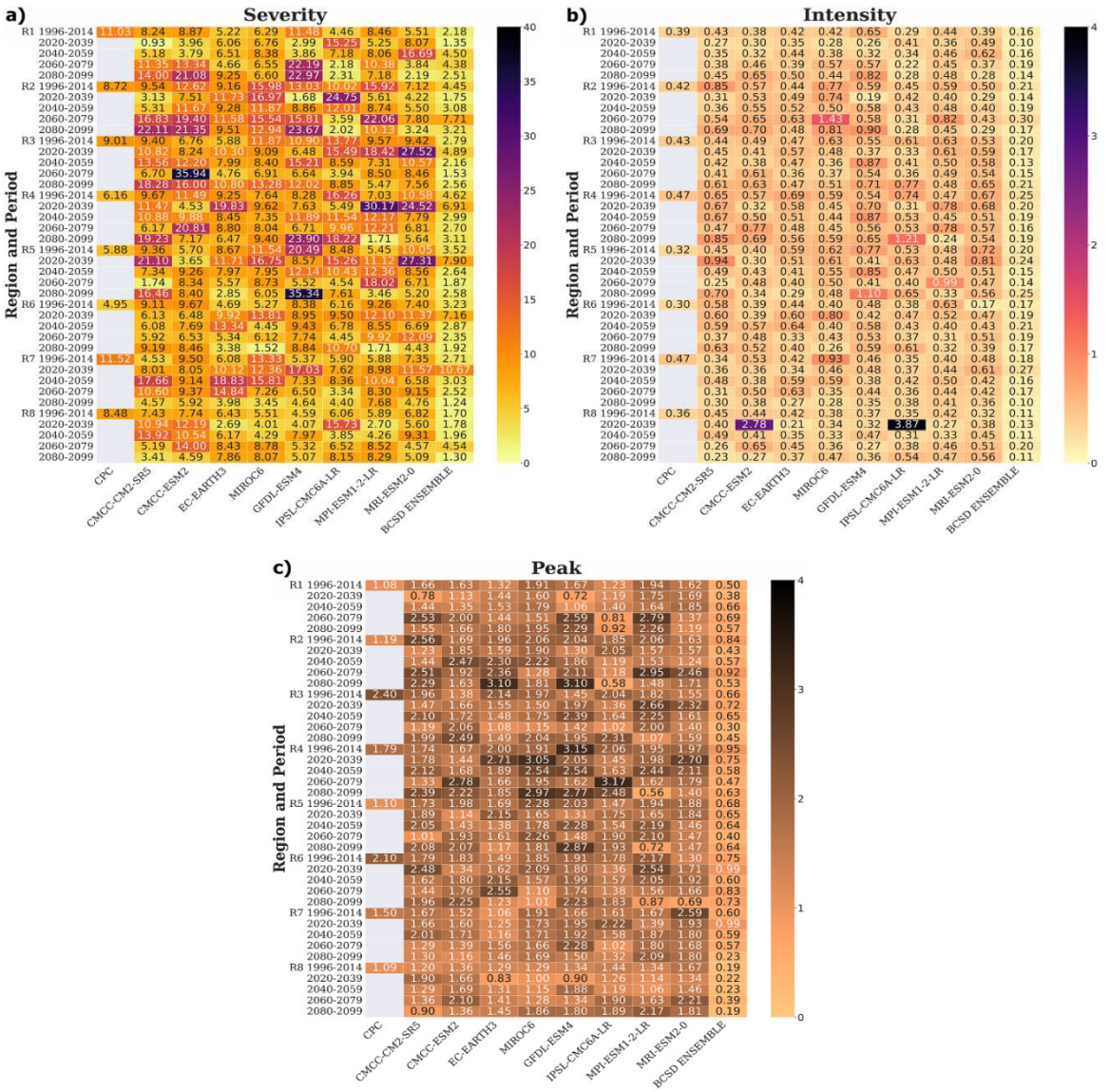

Figure 8. Heatmaps of drought severity (a), intensity (b), and peak (c) projected by the bias-corrected CMIP6-GCMs and BCSD ensemble under the SSP5-8.5 scenario for eight subdomains of SA.

For R1, of the 301 episodes identified by all datasets, 72% (218 cases) belong to the mild drought category, 16% (48 cases) correspond to the moderate drought class, 9% (28 cases) are of severe drought events, and 2% (7 cases) belong to the extreme drought category. Moreover, only three GCMs (CMCC-CM2-SR5, CMCC-ESM2, and MPI-ESM1-2-LR) indicate a slight increase in the average number of drought episodes in the 2020-2099 relative to the historical period, while the IPSL-CM6A-LR model and BCSD ensemble suggest a reduction of up to 27% and 23%, respectively.

On the other hand, seven of the nine datasets show an increase in the duration of drought episodes in 2020-2099 relative to 1996-2014. The IPSL-CM6A-LR and EC-Earth3 models indicate an increase of 47% and 32% in the duration (in months) of the events, respectively, while the BCSD ensemble provides an average increase of 25%. Similarly, most GCMs (and the BCSD ensemble) converge on increasing severity of drought episodes in the 21st century, with the IPSL-CM6A-LR model and the BCSD ensemble indicating increases of 51% and 40%, respectively. Regarding the intensity and peak parameters, GCMs show mixed signals, and the MRI-ESM2-0 and EC-Earth3 models show 12% and 18% increases in intensity and peak, respectively. In general, in this region, all GCMs overestimate the number of drought episodes over the historical period, and the GFDL-ESM4 and IPSL-CM6A-LR models show the largest range of parameter estimates for the 2020-2099 period.

 doi:10.20944/preprints202307.0373.v1

In R2, of the 252 episodes identified by all datasets, 65% (163 cases) correspond to the mild drought class, 17% (43 cases) are of moderate drought events, 12% (30 cases) refer to severe drought events, and 6% (16 cases) are of extreme drought events. Additionally, about 70% of the datasets converge to a growing number of drought episodes in the coming decades relative to 1996-2014, with the MPI-ESM1-2-LR and MRI-ESM2-0 models indicating an average increase of up to 45% and 38%, respectively. In addition, half of the datasets show an increase in drought duration in the 21st century, with the CMCC-CM2-SR5 model providing an average increase of up to 50%. Similarly, this model projects an average increase of 24% in the severity of drought episodes. For the intensity and peak parameters, the GCMs show mixed signals, with the EC-Earth3 model providing an average increase of up to 19% in the magnitude of both parameters. In general, in this region, the GCMs perform better in representing drought episodes during the historical period, with the CMCC-ESM2 and GFDL-ESM4 models providing the same number of episodes obtained by CPC.

In R3, 245 drought episodes were identified by the datasets, of which 64% (156 cases) correspond to mild drought episodes, 23% (56 cases) are moderate droughts, 9% (21 cases) are severe drought events, and 5% (12 cases) are extreme drought events. In this region, half of the datasets project an increase in the frequency of drought episodes in the 2020-2099 period (relative to 1996-2014), and half show a decrease. CMCC-ESM2 model indicates an average reduction of up to 47% in the number of episodes, but the MIROC6 model shows an average increase of up to 33%. Contrarily, only two GCMs (GFDL-ESM4 and IPSL-CM6A-LR) provide a reduction in episode duration, while all the others project increase during the following decades. MRI-ESM2-0 and CMCC-ESM2 yield average increases in the duration of drought episodes of up to 44% and 100%, respectively. These same models also provide the largest average increases in severity, corresponding to 44% and 168% (by MRI-ESM2-0 and CMCC-ESM2, respectively). As for the other regions, the intensity and peak projections show mixed signals, with the CMCC-ESM2 model indicating a 44% increase in the average peak magnitude of episodes in 2020-2099, while the EC-Earth3 model shows a 34% reduction.

For R4, 267 drought episodes were identified by all datasets, of which 58% (156 cases) were classified as mild droughts, 21% (57 cases) as moderate droughts, 11% (29 cases) as severe droughts, and 9% (25 cases) as extreme droughts. In this sector, GCMs show divergent projections about the frequency of drought episodes in 2020-2099. While the IPSL-CM6A-LR model projects an average increase of up to 50% in frequency, the MPI-ESM1-2-LR model estimates an average reduction of up to 43%. However, models converge about the increasing duration over the coming decades, with only three GCMs projecting reductions (CMCC-ESM2, IPSL-CM6A-LR, and MRI-ESM2-0) and the MPI-ESM1-2-LR model indicating an average increase of up to 61%. Similarly, GCMS are more homogenous in the increasing severity, with the MPI-ESM1-2-LR model providing an average increase of up to 100%. Whilst GCMs project mixed signals about changes in the intensity, projections of peak changes are more concordant, with most models indicating an increase. In this case, the MIROC6 model projects an average increase of up to 37% in peak episodes over the coming decades.

In R5, all datasets total 277 drought episodes, of which 64% (176 cases) correspond to the mild drought class, 21% (58 cases) are moderate drought events, 11% (31 cases) are severe drought events, and 4% (12 cases) are extreme drought events. In this region, more than half of the datasets project an increasing frequency in drought episodes in 2020-2099, with the GFDL-ESM4 model indicating an average increase of up to 63%, while the MPI-ESM1-2-LR model projects an average reduction of up to 46%. Similarly, the same proportion of models projects an increase in episode duration over the coming decades, with the CMCC-ESM2 and MPI-ESM1-2-LR models providing average increases of up to 40% and 90%, respectively.

Regarding severity, only three GCMs project a reduction (EC-Earth3, MIROC6, and GFDL-ESM4), and the MPI-ESM1-2-LR model estimates an average increase of up to 106%. For the intensity and peak parameters, the signals provided are heterogeneous, with projections of change in intensity ranging from -32% (by EC-Earth3) to 34% (by CMCC-CM2-SR5) and amplitude of change in peak from -17% (by MRI-ESM2-0) to 21% (by IPSL-CM6A-LR).

For R6, of the 324 episodes identified by the datasets, 70% (227 cases) were classified as mild droughts, 16% (51 cases) as moderate droughts, 12% (38 cases) as severe droughts, and 2% (8 cases)

as extreme droughts. In this sector, half of the ensembles project a reduction in the frequency of drought episodes (with the EC-Earth3 model providing an average reduction of up to 21%). Inversely, another half suggests an increase (with the CMCC-CM2-SR5 model projecting an average increase of up to 32%). Regarding episode duration in the 2020-2099 period, only two GCMs project a reduction (CMCC-CM2-SR5 and CMCC-ESM2), while the MIROC6 and EC-Earth3 models provide an average increase of 29% and 37%, respectively. Likewise, only three GCMs indicate a reduction in severity (CMCC-CM2-SR5, CMCC-ESM2, and MPI-ESM1-2-LR), while the IPSL-CM6A-LR and EC-Earth3 models project an average increase of 27% and 70%, respectively. Of the same, only the models CMCC-CM2-SR5 and MPI-ESM1-2-LR project a reduction in the intensity of drought episodes in 2020-2099, while the MRI-ESM2-0 model indicates an average increase of up to 158%. Regarding the peak of identified episodes, the outputs indicate mixed signals, with the EC-Earth3 model projecting an average increase of 26% and the MIROC6 model providing an average reduction of up to 22%.

In R7, a total of 293 drought episodes was obtained, with 70% (206 cases) being mild droughts, 19% (56 cases) of moderate droughts, 9% (27 cases) being severe droughts, and 1% (4 cases) of extreme droughts. Regarding the frequency, only two GCMs project an increase in the incidence (21% and 25% by the CMCC-ESM2 and MIROC6 models, respectively), while models such as EC-Earth3 and CMCC-CM2-SR5 indicate a reduction of 25% and 40%, respectively. Contrarily, only two GCMs project a reduction in episode duration (2% and 5% by CMCC-ESM2 and MIROC6 models, respectively), while EC-Earth3 and CMCC-CM2-SR5 models indicate a 49% and 101% increase, respectively. Alike, most models converge to a signal of increased severity of hydrological drought episodes in the region in 2020-2099, with the GFDL-ESM4, EC-Earth3, and CMCC-CM2-SR5 models projecting average increases of 65%, 96%, and 125%, respectively. The datasets indicate mixed signals for intensity, with decreases and increases ranging from 4% to 55% and 6% to 13%, respectively. Similarly, projections of change in episode peaks are also more heterogeneous, with reductions and increases ranging from 0.10% to 30% and 7% to 28%, respectively.

Finally, in R8, all datasets give a total of 331 drought episodes in 2020-2099, of which 81% (268 cases) are classified as mild droughts, 13% (43 cases) as moderate droughts, 5% (17 cases) as severe droughts, and 1% (3 cases) as extreme droughts. Half of the outputs project a reduction in the duration of episodes in the sector, while another indicates an increase. As for the other regions, most GCMs converge on a signal of increasing duration of drought episodes, with the GFDL-ESM4 model projecting an average increase of up to 34%. Likewise, projections among the models are more concordant about the increasing severity, with the IPSL-CMC6A-LR model providing an average increase of up to 41%. Additionally, most GCMs project an increase in peak episodes in 2020-2099 (only the EC-Earth3 model indicates an average reduction of up to 3%), with the BCSD ensemble providing an average increase of up to 32%.

In summary, GCMs project mixed signals about changes in drought events' frequency, intensity, and peak magnitudes during the coming decades in the SA subdomains. On the other hand, the projections are more homogeneous regarding the duration and severity of the episodes, with most models converging to increasing magnitudes of both parameters in all sectors evaluated. Concerning the different categories of droughts (mild, moderate, severe, and extreme), results show a larger occurrence of mild droughts. However, regions like the northern and central Northeast, Midwest, and Southeast Brazil show a substantial proportion (above 20%) of moderate drought events, as well as a relevant occurrence (above 10%) of severe drought events in the Amazonia region, central Northeast, Midwest, and Southeast Brazil. In this context, we highlight that although the BCSD ensemble provides predominantly mild drought episodes, individual analyses of the CMIP6-GCMs indicate expressive frequencies of moderate and severe events in all the evaluated subdomains.

4. Conclusions

In this study, we applied statistical downscaling to CMIP6 precipitation projections in SA using the CPC data as a reference to evaluate future changes in precipitation and the occurrence of hydrological droughts in the continent. To this end, we used the QDM technique developed by Cannon et al. [92], and the method proved effective in reducing systematic biases and preserving the

trends of GCMs' projections. For the coming decades, the post-processed precipitation projections indicated reduced rainfall in sectors such as northern SA, North, Northeast, Midwest, and Southeast Brazil and increased precipitation in southern Brazil and SESA regions. Such changes are more prominent during the austral spring (SON), and their signal is more robust under the SSP5-8.5 scenario, corroborating the literature.

The SPI-12 Index analysis showed considerable variability of projections among the GCMs about drought event parameters such as frequency, intensity, and peak. On the other hand, concerning duration and severity, a more remarkable agreement was observed among the GCMs regarding the intensification of both aspects in practically all the subdomains analyzed. Considering the different categories of drought events, the results showed a substantial frequency of moderate and severe droughts in the Northeast, Midwest, and Southeast Brazil. In addition, the individual CMIP6-GCMs and the BCSD ensemble project a considerable proportion of events with duration equal to or greater than 10 months in all evaluated South American sectors.

Given the results, it is valid to highlight some limitations of the study. Firstly, we point out that although the SPI-12 analysis is easy to implement because it uses only precipitation information, it disregards crucial aspects of the droughts related to temperature and evapotranspiration processes. In this context, analyses have indicated that the frequency and duration of droughts in SA are driven mainly by climate factors such as maximum and minimum temperatures, net surface radiation, and precipitation [145]. Thus, future studies employing statistical downscaling should address these aspects for assessing droughts on the continent during the 21st century.

Furthermore, although the study employed eight GCMs and the multi-model ensemble, it is recommended that future works use a larger number of models and forcing scenarios to minimize the uncertainties associated with the projections. Moreover, the projections presented here have an intermediate spatial resolution of 50 km, which limits the spatial detail of the analyses performed. In this sense, further research should consider climate projections with a finer spatial resolution to ensure greater accuracy of the results. However, the feasibility of such approaches demands high computational costs. Overall, despite the uncertainties associated with GCMs, the identification of hydrological drought episodes, and the bias correction technique, the results presented here can provide valuable subsidies to decision-makers and energy planners for better management of water resources in the South American continent for the coming decades.

Author Contributions: Conceptualisation, G.W.d.S.F. and M.S.R.; methodology, G.W.d.S.F. and M.S.R.; software, G.W.d.S.F., M.S.R., J.G.M.R. and C.A.d.S.; formal analysis, G.W.d.S.F. and M.S.R.; writing – original draft preparation, G.W.d.S.F. and M.S.R.; writing – review and editing, G.W.d.S.F. and M.S.R. All authors have read and agreed to the published version of the manuscript.

Funding: The authors thank the Coordination for the Improvement of Higher Education Personnel (CAPES, Finance Code 001), the National Council for Scientific and Technological Development (CNPq), and the R&D project from Engie Brazil Energy (R&D-00403-0054/2022) regulated by the Brazilian National Electric Energy Agency (ANEEL).

Institutional Review Board Statement: Not applicable.

Informed Consent Statement: Not applicable.

Data Availability Statement: All datasets used in this study are available on public online databases.

Acknowledgments: The authors thank the Coordination for the Improvement of Higher Education Personnel (CAPES), the Brazilian National Electric Energy Agency (ANEEL), the National Council for Scientific and Technological Development (CNPq), and the ENGIE Brazil Energy for the financial support. The authors also thank the Coupled Model Intercomparison Project (CMIP) and Climate Prediction Center (NOAA–CPC) for providing the datasets used in this study.

Conflicts of Interest: The authors declare no conflict of interest. The funders had no role in the design of the study; in the collection, analyses, or interpretation of the data; in the writing of the manuscript; or in the decision to publish the results.

References

1. Intergovernmental Panel on Climate Change (IPCC). Summary for Policymakers. In: Climate Change 2023: Synthesis Report. A Report of the Intergovernmental Panel on Climate Change. Contribution of Working Groups I, II and III to the Sixth Assessment Report of the Intergovernmental Panel on Climate Change [Core Writing Team, H. Lee and J. Romero (eds.)]. IPCC, Geneva, Switzerland, 2023, 36 pages. https://www.ipcc.ch/report/ar6/syr/downloads/report/IPCC_AR6_SYR_SPM.pdf
2. United Nations Environment Programme (UNEP). Emissions Gap Report 2022: The Closing Window – Climate crisis calls for rapid transformation of societies. Nairobi. 2022. https://www.unep.org/emissions-gap-report-2022
3. Tavares, P.S.; Acosta, R.; Nobre, P.; Resende, N.C.; Chou, S.C.; Lyra, A.A. Water balance components and climate extremes over Brazil under 1.5 °C and 2.0 °C of global warming scenarios. *Reg Environ Change* **2023**, *23*, 40. https://doi.org/10.1007/s10113-023-02042-1
4. Panisset, J.S.; Libonati, R.; Gouveia, C.M.P.; Machado-Silva, F.; França, D.A.; França, J.R.A.; Peres, L.F. Contrasting patterns of the extreme drought episodes of 2005, 2010 and 2015 in the Amazon Basin. *Int J Climatol* **2018**, *38*, 1096-1104. https://doi.org/10.1002/joc.5224
5. Gozzo, L.F.; Palma, D.S.; Custodio, M.S.; Machado, J.P. Climatology and trend of severe drought events in the state of Sao Paulo, Brazil, during the 20th century. *Atmosphere* **2019**, *10*, 190. https://doi.org/10.3390/atmos10040190
6. Gozzo, L.F.; Drumond, A.; Pampuch, L.A.; Ambrizzi, T.; Crespo, N.M.; Reboita, M.S.; Bier, A.A.; Carpenedo, C.B.; Bueno, P.G.; Pinheiro, H.R.; Custodio, M.S.; Kuki, C.A.C.; Tomaziello, A.C.N.; Gomes, H.B.; da Rocha, R.P.; Coelho, C.A.S..; Pimentel, R.M. Intraseasonal drivers of the 2018 drought over São Paulo, Brazil. *Front Clim* **2022**, *4*. https://doi.org/10.3389/fclim.2022.852824
7. Papalexiou, S.M.; Rajulapati, C.R.; Andreadis, K.M.; Foufoula-Georgiou, E.; Clark, M.P.; Trenberth, K.E. Probabilistic Evaluation of drought in CMIP6 simulations. *Earth's Future* **2021**, *9*, e2021EF002150. https://doi.org/10.1029/2021EF002150
8. Medeiros, F.J.; Oliveira, C.P. Assessment of dry and heavy rainfall days and their projected changes over Northeast Brazil in Coupled Model Intercomparison Project Phase 6 models. *Int J Climatol* **2022**, *42*, 8665-8686. https://doi.org/10.1002/joc.7759
9. Keellings, D.; Engström, J. The future of drought in the southeastern U.S.: Projections from downscaled CMIP5 models. *Water* **2019**, *11*, 259. https://doi.org/10.3390/w11020259
10. Swain, S.; Hayhoe, K. CMIP5 projected changes in spring and summer drought and wet conditions over North America. *Clim Dyn* **2015**, *44*, 2737-2750. https://doi.org/10.1007/s00382-014-2255-9
11. Cook, B.I.; Mankin, J.S.; Marvel, K.; Williams, A.P.; Smerdon, J.E.; Anchukaitis, K.J. Twenty-first century drought projections in the CMIP6 forcing scenarios. *Earth's Future* **2020**, *8*, e2019EF001461. https://doi.org/10.1029/2019EF001461
12. Wu, C.; Yeh, P.J.-F.; Chen, Y.-Y.; Lv, W.; Hu, B.X.; Huang, G. Future precipitation-driven meteorological drought changes in the CMIP5 multimodel ensembles under 1.5 °C and 2 °C global warming. *J Hydrometeorol* **2020**, *21*, 2177-2196. https://doi.org/10.1175/JHM-D-19-0299.1
13. Wu, C.; Yeh, P.J.-F.; Chen, Y.-Y.; Lv, W.; Hu, B.X.; Huang, G. Copula-based risk evaluation of global meteorological drought in the 21st century based on CMIP5 multi-model ensemble projections. *J Hydrol* **2021**, *598*, 126265. https://doi.org/10.1016/j.jhydrol.2021.126265
14. Wang, T.; Tu, X.; Singh, V.P.; Chen, X.; Lin, K. Global data assessment and analysis of drought characteristics based on CMIP6. *J Hydrol* **2021**, *596*, 126091. https://doi.org/10.1016/j.jhydrol.2021.126091
15. Tam, B.Y.; Szeto, K.; Bonsal, B.; Flato, G.; Cannon, A.J.; Rong, R. CMIP5 drought projections in Canada based on the Standardized Precipitation Evapotranspiration Index. *Can Water Resour J* **2019**, *44*, 90-107. https://doi.org/10.1080/07011784.2018.1537812
16. Javadinejad, S.; Hannah, D.; Ostad-Ali-Askari, K.; Krause, S.; Zalewski, M.; Boogaard, F. The impact of future climate change and human activities on hydro-climatological drought, analysis and projections: Using CMIP5 climate model simulations. *Water Conserv Sci Eng* **2019**, *4*, 71-88. https://doi.org/10.1007/s41101-019-00069-2
17. Nguyen-Ngoc-Bich, P.; Phan-Van, T.; Ngo-Duc, T.; Vu-Minh, T.; Trinh-Tuan, L.; Tangang, F.T.; Juneng, L.; Cruz, F.; Santisirisomboon, J.; Narisma, G.; Aldrian, E. Projected evolution of drought characteristics in Vietnam based on CORDEX-SEA downscaled CMIP5 data. *Int J Climatol* **2021**, *41*, 5733-5751. https://doi.org/10.1002/joc.7150
18. Coppola, E.; Raffaele, F.; Giorgi, F.; Giuliani, G.; Xuejie, G.; Ciarlo, J.M.; Sines, T.R.; Torres-Alavez J.A.; Das, S.; di Sante, F.; Pichelli, E.; Glazer, R.; Müller, S.K.; Omar, S.A.; Ashfaq, M.; Bukovsky, M.; Im, E.-S.; Jacob, D.; Teichmann, C.; Remedio, A.; Remke, T.; Kriegsmann, A.; Bülow, K.; Weber, T.; Buntemeyer, L.; Sieck, K.; Rechid, D. Climate hazard indices projections based on CORDEX-CORE, CMIP5 and CMIP6 ensemble. *Clim Dyn* **2020**, *57*, 1293-1383. https://doi.org/10.1007/s00382-021-05640-z

19. Bouramdane, A.-A. Assessment of CMIP6 multi-model projections worldwide: Which regions are getting warmer and are going through a drought in Africa and Morocco? What changes from CMIP5 to CMIP6? *Sustainability* **2023**, *15*, 690. https://doi.org/10.3390/su15010690
20. Betts, R.A.; Alfieri, L.; Bradshaw, C.; Caesar, J.; Feyen, L.; Friedlingstein, P.; Gohar, L.; Koutroulis, A.; Lewis, K.; Morfopoulos, C.; Papadimitriou, L.; Richardson, K.J.; Tsanis, I.; Wyser, K. Changes in climate extremes, fresh water availability and vulnerability to food insecurity projected at 1.5 °C and 2 °C global warming with a higher-resolution global climate model. *Phil Trans R Soc A* **2018**, *376*, 20160452. https://doi.org/10.1098/rsta.2016.0452
21. Campozano, L.; Ballari, D.; Montenegro, M.; Avilés, A. Future meteorological droughts in Ecuador: Decreasing trends and associated spatio-temporal features derived from CMIP5 models. *Front Earth Sci* **2020**, *8*. https://doi.org/10.3389/feart.2020.00017
22. Marengo, J.A.; Cunha, A.P.M.A.; Nobre, C.A.; Ribeiro Neto, G.G.; Magalhaes, A.R.; Torres, R.R.; Sampaio, G.; Alexandre, F.; Alves, L.M.; Cuartas, L.A.; Deusdará, K.R.L.; Álvala, R.C.S. Assessing drought in the drylands of northeast Brazil under regional warming exceeding 4 °C. *Nat Hazards* **2020**, *103*, 2589-2611. https://doi.org/10.1007/s11069-020-04097-3
23. Reboita, M.S.; Kuki, C.A.C.; Marrafon, V.H.; Souza, C.A.; Ferreira, G.W.S.; Teodoro, T.; Lima, J.W.M. South America climate change revealed through climate indices projected by GCMs and Eta-RCM ensembles. *Clim Dyn* **2021**, *58*, 459-485. https://doi.org/10.1007/s00382-021-05918-2
24. Reboita, M.S.; da Rocha, R.P.; Souza, C.A.; Baldoni, T.C.; Silva, P.L.L.S.; Ferreira, G.W.S. Future projections of extreme precipitation climate indices over South America based on CORDEX-CORE multimodel ensemble. *Atmosphere* **2022**, *13*, 1463. https://doi.org/10.3390/atmos13091463
25. Gouveia, C.D.; Torres, R.R.; Marengo, J.A.; Avila-Diaz, A. Uncertainties in projections of climate extremes indices in South America via Bayesian inference. *Int J Climatol* **2022**, *42*, 7362-7382. https://doi.org/10.1002/joc.7650
26. Marengo, J.A.; Alves, L.M.; Alvala, R.C.S.; Cunha, A.P.; Brito, S.; Moraes, O.L.L. Climatic characteristics of the 2010-2016 drought in the semi-arid Northeast Brazil region. *An Acad Bras Ciênc* **2018**, *90*, 1973-1985. https://doi.org/10.1590/0001-3765201720170206
27. Marengo, J.A.; Torres, R.R.; Alves, L.M. Drought in Northeast Brazil: Past, present, and future. *Theor Appl Climatol* **2016**, *129*, 1189-1200. https://doi.org/10.1007/s00704-016-1840-8
28. Marengo, J.A.; Galdos, M.V.; Challinor, A.; Cunha, A.P.; Marin, F.R.; Vianna, M.S.; Alvala, R.C.S.; Alves, L.M.; Moraes, O.L.; Bender, F. Drought in Northeast Brazil: A review of agricultural and policy adaptation options for food security. *Climate Res Sustain* **2022**, *1*, e17. https://doi.org/10.1002/cli2.17
29. Cavalcanti, I.F.A.; Kousky, V.E. Drought in Brazil during summer and fall 2001 and associated atmospheric circulation features. *Revista Climanálise* **2001**, 1. http://climanalise.cptec.inpe.br/~rclimanl/revista/pdf/criseing.pdf
30. Seth, A.; Fernandes, K.; Camargo, S.J. Two summers of São Paulo drought: Origins in the western tropical Pacific. *Geophys Res Lett* **2015**, *42*, 10816-10823. https://doi.org/10.1002/2015GL066314
31. Nobre, C.A.; Marengo, J.A; Seluchi, M.E.; Cuartas, A.; Alves, L.M. Some characteristics and impacts of the drought and water Crisis in southeastern Brazil during 2014 and 2015. *J Water Resour Prot* **2016**, *8*, 252-262. http://dx.doi.org/10.4236/jwarp.2016.82022
32. Coelho, C.A.S.; Oliveira, C.P.; Ambrizzi, T.; Reboita, M.S.; Carpenedo, C.B.; Campos, J.L.P.S.; Tomaziello, A.C.N.; Pampuch, L.A.; Custódio, M.S.; Dutra, L.M.M.; da Rocha, R.P.; Rehbein, A. The 2014 southeast Brazil austral summer drought: regional scale mechanisms and teleconnections. *Clim Dyn* **2016**, *46*, 3737-3752. https://doi.org/10.1007/s00382-015-2800-1
33. Abatan, A.A.; Tett, S.F.B.; Dong, B.; Cunningham, C.; Rudorff, C.M.; Klingaman, N.P.; de Abreu, R.C. Drivers and physical processes of drought events over the state of São Paulo, Brazil. *Clim Dyn* **2022**, *58*, 3105-3119. https://doi.org/10.1007/s00382-021-06091-2
34. Geirinhas, J.L.; Russo, A.C.; Libonati, R.; Miralles, D.G.; Sousa, P.M.; Wouters, H.; Trigo, R.M. The influence of soil dry-out on the record-breaking hot 2013/2014 summer in Southeast Brazil. *Sci Reports* **2022**, *12*, 5836. https://doi.org/10.1038/s41598-022-09515-z
35. Cuartas, L.A.; Cunha, A.P.M.A.; Alves, J.A.; Parra, L.M.P.; Deusdará-Leal, K.; Costa, L.C.O.; Molina, R.D.; Amore, D.; Broedel, E.; Seluchi, M.E.; Cunningham, C.; Alvalá, R.C.S.; Marengo, J.A. Recent hydrological droughts in Brazil and their impact on hydropower generation. *Water* **2022**, *14*, 601. https://doi.org/10.3390/w14040601
36. Coelho, C.A.S.; Cardoso, D.H.F.; Firpo, M.A.F. Precipitation diagnostics of an exceptionally dry event in São Paulo, Brazil. *Theor Appl Climatol* **2016**, *125*, 769-784. https://doi.org/10.1007/s00704-015-1540-9
37. Marengo, J.A.; Espinoza, J.C. Extreme seasonal droughts and floods in Amazonia: Causes, trends and impacts. *Int J Climatol* **2016**, *36*, 1033-1050. https://doi.org/10.1002/joc.4420
38. Agudelo, J.; Arias, P.A.; Vieira, S.C.; Martínez, J.A. Influence of longer dry seasons in the Southern Amazon on patterns of water vapor transport over northern South America and the Caribbean. *Clim Dyn* **2019**, *52*, 2647-2665. https://doi.org/10.1007/s00382-018-4285-1

39. Lovejoy, T.E.; Nobre, C. Amazon tipping point: Last chance for action. *Sci Adv* **2019**, *5*, eaba2949. https://www.science.org/doi/10.1126/sciadv.aba2949
40. Jimenez, J.C.; Marengo, J.A.; Alves, L.M.; Sulca, J.C.; Takahashi, K.; Ferrett, S.; Collins, M. The role of ENSO flavours and TNA on recent droughts over Amazon forests and the Northeast Brazil region. *Int J Climatol* **2021**, *41*, 3761-3780. https://doi.org/10.1002/joc.6453
41. Guimberteau, M.; Ronchail, J.; Espinoza, J.C.; Lengaigne, M.; Sultan, B.; Polcher, J.; Drapeau, G.; Guyot, J.-L.; Ducharne, A.; Ciais, P. Future changes in precipitation and impacts on extreme streamflow over Amazonian sub-basins. *Environ Res Lett* **2013**, *8*, 014035. https://iopscience.iop.org/article/10.1088/1748-9326/8/1/014035
42. Duffy, P.B.; Brando, P.; Asner, G.P.; Field, C.B. Projections of future meteorological drought and wet periods in the Amazon. *Proc Natl Acad Sci USA* **2015**, *112*, 43. https://doi.org/10.1073/pnas.1421010112
43. Boulton, C.A.; Lenton, T.M.; Boers, N. Pronounced loss of Amazon rainforest resilience since the early 2000s. *Nat Clim Chang* **2022**, *12*, 271-278. https://doi.org/10.1038/s41558-022-01287-8
44. Borges, P.A.; Bernhofer, C.; Rodrigues, R. Extreme rainfall indices in Distrito Federal, Brazil: Trends and links with El Niño southern oscillation and Madden–Julian oscillation. *Int J Climatol* **2018**, *38*, 4550-4567. https://doi.org/10.1002/joc.5686
45. Thielen, D.; Schuchmann K.-L.; Ramoni-Perazzi, P.; Marquez, M.; Rojas, W.; Quintero, J.I.; Marques, M.I. Quo vadis Pantanal? Expected precipitation extremes and drought dynamics from changing sea surface temperature. *PLoS ONE* **2020**, *15*, e0227437. https://doi.org/10.1371/journal.%20pone.0227437
46. Marengo, J.A.; Cunha, A.P.; Cuartas, L.A.; Deusdará-Leal, K.R.; Broedel, E.; Seluchi, M.E.; Michelin, C.M.; Baião, C.F.P.; Ângulo, E.C.; Almeida, E.K.; Kazmierczak, M.L.; Mateus, N.P.A.; Silva, R.C.; Bender, F. Extreme drought in the Brazilian Pantanal in 2019–2020: Characterization, causes, and impacts. *Front Water* **2021**, *3*. https://doi.org/10.3389/frwa.2021.639204
47. Cunha, A.P.M.A.; Zeri, M.; Deusdará-Leal, K.; Costa, L.; Cuartas, L.A.; Marengo, J.A.; Tomasella, J.; Vieira, R.M.; Barbosa, A.A.; Cunningham, C.; Garcia, J.V.C.; Broedel, E.; Alvalá, R.; Ribeiro-Neto, R. Extreme drought events over Brazil from 2011 to 2019. *Atmosphere* **2019**, *10*, 642. https://doi.org/10.3390/atmos10110642
48. Fernandes, V.R.; Cunha, A.P.M.A.; Pineda, L.A.C.; Leal, K.R.D.; Costa, L.C.O.; Broedel, E.; França, D.A.; Alvalá, R.C.S.; Seluchi, M.E.; Marengo, J.A. Secas e os impactos na região sul do Brasil. *Rev Bras Climatol* **2021**, *28*, 561-584. http://dx.doi.org/10.5380/rbclima.v28i0.74717
49. Müller, O.V.; Berbery, E.H.; Alcaraz-Segura, D.; Ek, M.B. Regional model simulations of the 2008 drought in southern South America using a consistent set of land surface properties. *J Clim* **2014**, *27*, 6754-6778. https://doi.org/10.1175/JCLI-D-13-00463.1
50. Sgroi, L.C.; Lovino, M.A.; Berbery, E.H.; Müller, G.V. Characteristics of droughts in Argentina's core crop region. *Hydrol Earth Syst Sci* **2021**, *25*, 2475-2490. https://doi.org/10.5194/hess-25-2475-2021
51. Lovino, M.A.; Müller, O.V.; Berbery, E.H.; Müller, G.V. How have daily climate extremes changed in the recent past over northeastern Argentina? *Glob Planet Change* **2018**, *168*, 78-97. https://doi.org/10.1016/j.gloplacha.2018.06.008
52. Olmo, M.; Bettolli, M.L.; Rusticucci, M. Atmospheric circulation influence on temperature and precipitation individual and compound daily extreme events: Spatial variability and trends over southern South America. *Weather Clim Extremes* **2020**, *29*, 100267. https://doi.org/10.1016/j.wace.2020.100267
53. Lovino, M.A.; Müller, G.V.; Pierrestegui, M.J.; Espinosa, E.; Rodríguez, L. Extreme precipitation events in the Austral Chaco region of Argentina. *Int J Climatol* **2022**, *42*, 5985-6006. https://doi.org/10.1002/joc.7572
54. Collazo, S. Barrucand, M.; Rusticucci, M. Evaluation of CMIP6 models in the representation of observed extreme temperature indices trends in South America. *Clim Change* **2022**, *172*, 21. https://doi.org/10.1007/s10584-022-03376-1
55. Balmaceda-Huarte, R.; Olmo, M.E.; Bettolli, M.L.; Poggi, M.M. Evaluation of multiple reanalyses in reproducing the spatio-temporal variability of temperature and precipitation indices over southern South America. *Int J Climatol* **2021**, *41*, 5572-5595. https://doi.org/10.1002/joc.7142
56. Freitas, A.A.; Reboita, M.S.; Carvalho, V.S.B.; Drumond, A.; Ferraz, S.E.T.; Silva, B.C.; da Rocha, R.P. Atmospheric and oceanic patterns associated with extreme drought events over the Paraná Hydrographic Region, Brazil. *Climate* **2023**, *11*, 12. https://doi.org/10.3390/cli11010012
57. McKee, T.B.; Doesken, N.J.; Kleist, J. The relationship of drought frequency and duration to time scales. In Proceedings of the 8th Conference on Applied Climatology; 1993; pp. 179–183. Available online: https://climate.colostate.edu/pdfs/relationshipofdroughtfrequency.pdf
58. Freitas, A.A.; Drumond, A.; Carvalho, V.S.B.; Reboita, M.S.; Silva, B.C.; Uvo, C.B. Drought assessment in São Francisco River Basin, Brazil: Characterization through SPI and associated anomalous climate patterns. *Atmosphere* **2022**, *13*, 41. https://doi.org/10.3390/atmos13010041
59. World Meteorological Organization (WMO). Standardized Precipitation Index user guide. WMO-No. 1090, 2012, Geneva.

60. Brito, S.S.B.; Cunha, A.P.M.; Cunningham, C.C.; Alvalá, R.C.; Marengo, J.A.; Carvalho, M.A. Frequency, duration and severity of drought in the Semiarid Northeast Brazil region. *Int J Climatol* **2017**, *38*, 517–529. https://doi.org/10.1002/joc.5225
61. Santos, S.R.Q.; Braga, C.C.; Sansigolo, C.A.; Santos, A.P.P. Determinação de regiões homogêneas do índice de precipitação normalizada (SPI) na Amazônia Oriental. *Rev Bras Meteorol* **2017**, 32, 111-122. http://dx.doi.org/10.1590/0102-778632120160013
62. Oliveira-Júnior, J.F.; Gois, G.; Terassi, P.M.B.; Silva Junior, C.A.; Blanco, C.J.C.; Sobral, B.S.; Gasparini, K.A.C. Drought severity based on the SPI index and its relation to the ENSO and PDO climatic variability modes in the regions North and Northwest of the State of Rio de Janeiro-Brazil. *Atmos Res* **2018**, *212*, 91-105. https://doi.org/10.1016/j.atmosres.2018.04.022
63. Pereira, V.R.; Blain, G.C.; Avila, A.M.; Pires, R.C.; Pinto, H.S. Impacts of climate change on drought: Changes to drier conditions at the beginning of the crop growing season in southern Brazil. *Bragantia* **2018**, *77*, 201-211. https://doi.org/10.1590/1678-4499.2017007
64. Cunha, A.P.M.A.; Zeri, M.; Leal, K.D.; Costa, L.; Cuartas, L.A.; Marengo, J.A.; Tomasella, J.; Vieira, R.M.; Barbosa, A.A.; Cunningham, C.; Garcia, J.V.C.; Broedel, E.; Alvalá, R.; Ribeiro-Neto, G. Extreme drought events over Brazil from 2011 to 2019. *Atmosphere* **2019**, *10*, 642. https://doi.org/10.3390/atmos10110642
65. Costa, M.D.S.; Oliveira-Júnior, J.F.D.; Santos, P.J.D.; Correia Filho,W.L.F.; Gois, G.D.; Blanco, C.J.C.; Teodoro, P.E.; Silva Junior, C.A.; Santiago, D.B.; Souza, E.O.; Jardim, A.M.R.F.. Rainfall extremes and drought in Northeast Brazil and its relationship with El Niño–Southern Oscillation. *Int J Climatol* **2020**, *41*, E2111–E2135. https://doi.org/10.1002/joc.6835
66. Silva, D.F.; Lima, M.J.S.; Souza Neto, P.F.; Gomes, H.B.; Silva, F.D.S.; Almeida, H.R.R.C.; Pereira, M.P.S.; Costa, R.L. Caracterização de eventos extremos e de suas causas climáticas com base no índice padronizado de precipitação para o leste do Nordeste. *Rev Bras Geogr Fis* **2020**, *13*, 449-464. https://doi.org/10.26848/rbgf.v13.2.p449-464
67. Xavier, L.C.P.; Silva, S.M.O.D.; Carvalho, T.M.N.; Pontes Filho, J.D.; Souza Filho, F.D.A.D. Use of machine learning in evaluation of drought perception in irrigated agriculture: The case of an irrigated perimeter in Brazil. *Water* **2020**, *12*, 1546. https://doi.org/10.3390/w12061546
68. Avila-Diaz, A.; Torres, R.R.; Zuluaga, C.F.; Cerón, W.L.; Oliveira, L.; Benezoli, V.; Rivera, I.A.; Marengo, J.A.; Wilson, A.B.; Medeiros, F. Current and future climate extremes over Latin America and Caribbean: Assessing Earth System Models from High Resolution Model Intercomparison Project (HighResMIP). *Earth Syst Environ* **2023**, *7*, 99-130. https://doi.org/10.1007/s41748-022-00337-7
69. Eyring, V.; Bony, S.; Meehl, G.A.; Senior, C.A.; Stevens, B.; Stouffler, R.J.; Taylor, K.E. Overview of the global coupled model intercomparison project phase 6 (CMIP6) experimental design and organization. *Geosci Model Dev* **2016**, *9*, 1937-1958. https://doi.org/10.5194/gmd-9-1937-2016
70. Riahi, K.; van Vuuren, D.P.; Kriegler, E.; Edmonds, J.; O'Neill, B.C.; Fujimori, S.; Bauer, N.; Calvin, K.; Dellink, R.; Fricko, O.; Lutz, W.; Popp, A.; Cuaresma, J.C.; Samir, K.C.; Leimbach, M.; Jiang, L.; Kram, T.; Rao, S.; Emmerling, J.; Ebi, K.; Hasegawa, T.; Havlik, P.; Humpenöder, F.; da Silva, L.A.; Smith, S.; Stehfest, E.; Bosetti, V.; Eom, J.; Gernaat, D.; Masui, T.; Rogelj, J.; Strefler, J.; Drouet, L.; Krey, V.; Luderer, G.; Harmsen, M.; Takahashi, K.; Baumstark, L.; Doelman, J.C.; Kainuma, M.; Klimont, Z.; Marangoni, G.; Lotze-Campen, H.; Obersteiner, M.; Tabeau, A.; Tavoni, M. The Shared Socio-economic Pathways and their energy, land use, and greenhouse gas emissions implications: A review. *Glob Environ Change* **2017**, *42*, 153-168. http://dx.doi.org/10.1016/j.gloenvcha.2016.05.009
71. Carvalho, D.; Rocha, A.; Costoya, X.; de Castro, M.; Gómez-Gesteira, M. Wind energy resource over Europe under CMIP6 future climate projections: What changes from CMIP5 to CMIP6. *Renew Sustain Energy Rev* **2021**, *151*, 111594. https://doi.org/10.1016/j.rser.2021.111594
72. Fowler, H.J.; Blenkisop, S.; Tebaldi, C. Linking climate change modelling to impacts studies: recent advances in downscaling techniques for hydrological modelling. *Int J Climatol* **2007**, *27*, 1547-1578. https://doi.org/10.1002/joc.1556
73. Ambrizzi, T.; Reboita, M.S.; da Rocha, R.P.; Llopart, M. The state of the art and fundamental aspects of regional climate modeling in South America. *Ann NY Acad Sci* **2019**, *1436*, 98-120. https://doi.org/10.1111/nyas.13932
74. Mutz, S.G.; Scherrer, S.; Muceniece, I.; Ehlers, T.A. Twenty-first century regional temperature response in Chile based on empirical-statistical downscaling. *Clim Dyn* **2021**, *56*, 2881-2894. https://doi.org/10.1007/s00382-020-05620-9
75. da Rocha, R.P.; Morales, C.A.; Cuadra, S.V.; Ambrizzi, T. Precipitation diurnal cycle and summer climatology assessment over South America: An evaluation of Regional Climate Model version 3 simulations. *J Geophys Res Atmos* **2009**, *114*, D10. https://doi.org/10.1029/2008JD010212
76. Marengo, J.A.; Chou, S.C.; Kay, G.; Alves, L.M.; Pesquero, J.F.; Soares, W.R.; Santos, D.C., Lyra, A.A.; Sueiro, G.; Betts, R.; Chagas, D.J.; Gomes, J.L.; Bustamante, J.F.; Tavares, P. Development of regional future climate change scenarios in South America using the Eta CPTEC/HadCM3 climate change projections:

Climatology and regional analyses for the Amazon, São Francisco and the Paraná River basins. *Clim Dyn* **2012**, *38*, 1829-1848. https://doi.org/10.1007/s00382-011-1155-5

77. Chou, S.C.; Lyra, A.; Mourão, C.; Dereczynski, C.; Pilotto, I.; Gomes, J.; Bustamante, J.; Tavares, P.; Silva, A.; Rodrigues, D.; Campos, D.; Chagas, D.; Sueiro, G.; Siqueira, G.; Nobre, P.; Marengo, J. Evaluation of the Eta simulations nested in three global climate models. *Am J Clim Change* **2014**, *3*, 438-454. https://doi.org/10.4236/AJCC.2014.35039
78. Reboita, M.S.; da Rocha, R.P.; Dias, C.G.; Ynoue, R.Y. Climate projections for South America: RegCM3 driven by HadCM3 and ECHAM5. *Adv Meteorol* **2014**, *2014*, 376738. http://dx.doi.org/10.1155/2014/376738
79. Reboita, M.S.; Dutra, L.M.M.; Dias, C.G. Diurnal cycle of precipitation simulated by RegCM4 over South America: Present and future scenarios. *Clim Res* **2016**, *70*, 39-55. https://doi.org/10.3354/cr01416
80. Reboita, M.S.; Amaro, T.R.; de Souza, M.R. Winds: Intensity and power density simulated by RegCM4 over South America in present and future climate. *Clim Dyn* **2018**, *51*, 187-205. https://doi.org/10.1007/s00382-017-3913-5
81. Solman, S.A.; Blázquez, J. Multiscale precipitation variability over South America: Analysis of the added value of CORDEX RCM simulations. *Clim Dyn* **2019**, *53*, 1547-1565. https://doi.org/10.1007/s00382-019-04689-1
82. Dereczynski, C.; Chou, S.C.; Lyra, A.; Sondermann, M.; Regoto, P.; Tavares, P.; Chagas, D.; Gomes, J.L.; Rodrigues, D.C.; Skansi, M.M. Downscaling of climate extremes over South America – Part I: Model evaluation in the reference climate. *Weather Clim Extremes* **2020**, *29*, 100273. https://doi.org/10.1016/j.wace.2020.100273
83. Solman, S.A.; Bettolli, M.L.; Doyle, M.E.; Olmo, M.E.; Feijoo, M.; Martinez, D.; Blázquez, J.; Balmaceda-Huarte, R. Evaluation of multiple downscaling tools for simulating extreme precipitation events over southeastern South America: A case study approach. *Clim Dyn* **2021**, *57*, 1241-1264. https://doi.org/10.1007/s00382-021-05770-4
84. Silva, N.P.; Crespo, N.M.; Kaufmann, C.L.G.; Lima, J.A.M.; Andrioni, M.; Camargo, R.; da Rocha, R.P. Adjustment of extreme wind speed in regional climate downscaling over southwestern South Atlantic. *Int J Climatol* **2022**, *42*, 9994-10008. https://doi.org/10.1002/joc.7876
85. Silva, M.L.; Oliveira, C.P.; Silva, C.M.S.; Araújo, J.M. Dynamic downscaling of climate simulations and projected changes in tropical South America using RegCM4.7. *Int J Climatol* **2023**, *Early View*. https://doi.org/10.1002/joc.8035
86. Bettolli, M.L.; Penalba, O.C. Statistical downscaling of daily precipitation and temperatures in southern La Plata Basin. *Int J Climatol* **2018**, *38*, 3705-3722. https://doi.org/10.1002/joc.5531
87. Sulca, J.; Vuille, M.; Timm, O.E.; Dong, B.; Zubieta, R. Empirical–statistical downscaling of austral summer precipitation over South America, with a focus on the Central Peruvian Andes and the Equatorial Amazon Basin. *J Appl Meteorol Climatol* **2021**, *60*, 65-85. https://doi.org/10.1175/JAMC-D-20-0066.1
88. Balmaceda-Huarte, R.; Bettolli, M.L. Assessing statistical downscaling in Argentina: Daily maximum and minimum temperatures. *Int J Climatol* **2022**, *42*, 8423-8445. https://doi.org/10.1002/joc.7733
89. Olmo, M.E.; Bettolli, M.L. Statistical downscaling of daily precipitation over southeastern South America: Assessing the performance in extreme events. *Int J Climatol* **2022**, *42*, 1283-1302. https://doi.org/10.1002/joc.7303
90. Olmo, M.E.; Balmaceda-Huarte, R.; Bettolli, M.L. Multi-model ensemble of statistically downscaled GCMs over southeastern South America: historical evaluation and future projections of daily precipitation with focus on extremes. *Clim Dyn* **2022**, *59*, 3051-3068. https://doi.org/10.1007/s00382-022-06236-x
91. Ballarin, A.S.; Sone, J.S.; Gesualdo, G.C.; Schwamback, D.; Reis, A.; Almagro, A.; Wendland, E.C. CLIMBra – Climate change dataset for Brazil. *Sci Data* **2023**, *10*, 47. https://doi.org/10.1038/s41597-023-01956-z
92. Cannon, A.J.; Sobie, S.R.; Murdock, T.Q. Bias correction of GCM precipitation by Quantile Mapping: How well do methods preserve changes in quantiles and extremes? *J Clim* **2015**, *28*, 6938–6959. https://doi.org/10.1175/JCLI-D-14-00754.1
93. Reboita, M.S.; Gan, M.A.; da Rocha, R.P.; Ambrizzi, T. Regimes de precipitação na América do Sul: uma revisão bibliográfica. *Rev. Bras. Meteorol.* **2010**, *25*, 185-204. https://doi.org/10.1590/S0102-77862010000200004
94. Ferreira, G.W.S.; Reboita, M.S. A new look into the South American precipitation patterns: Observation and forecast. *Atmosphere* **2022**, *13*, 873. https://doi.org/10.3390/atmos13060873.
95. Zhou J.; Lau, K.M. Does a monsoon climate exist over South America? J Clim **1998**, 11, 1020-1040. https://doi.org/10.1175/1520-0442(1998)011%3C1020:DAMCEO%3E2.0.CO;2
96. Hoyos, I.; Cañón-Barriga, J.; Arenas-Suárez, T.; Dominguez, F.; Rodríguez, B.A. Variability of regional atmospheric moisture over Northern South America: patterns and underlying phenomena. Clim Dyn **2019**, 52, 893-911. https://doi.org/10.1007/s00382-018-4172-9
97. Mejía, J.F.; Yepes, J.; Henao, J.J.; Poveda, G.; Zuluaga, M.D.; Raymond, D.J.; Fuchs-Stone, Z. Towards a mechanistic understanding of precipitation over the far eastern tropical Pacific and western Colombia, one

of the rainiest spots on Earth. J Geophys Res Atmos **2021**, 126, e2020JD033415. https://doi.org/10.1029/2020JD033415

98. Lagos-Zúñiga, M.A.; Balmaceda-Huarte, R.; Regoto, P.; Torrez, L.; Olmo, M.; Lyra, A.; Pareja-Quispe, D.; Bettolli, M.L. Extreme indices of temperature and precipitation in South America: Trends and intercomparison of regional climate models. Clim Dyn (Under Review). https://doi.org/10.21203/rs.3.rs-1717139/v1
99. Rupp, D.E.; Abatzoglou, J.T.; Hegewisch, K.C.; Mote, P.W. Evaluation of CMIP5 20th century climate simulations for the Pacific Northwest USA. *J Geophys Res Atmos* **2013**, *118*, 10884-10906. https://doi.org/10.1002/jgrd.50843
100. Dias, C.G.; Reboita, M.S. Assessment of CMIP6 simulations over tropical South America. *Rev Bras Geogr Fis* **2021**, *14*, 1282-1295. https://doi.org/10.26848/rbgf.v14.3.p1282-1295
101. Zhang, M.Z.; Xu, Z.; Han, Y.; Guo, W. Evaluation of CMIP6 models toward dynamical downscaling over 14 CORDEX domains. *Clim Dyn* **2022**. https://doi.org/10.1007/s00382-022-06355-5
102. Lovato, T.; Peano, D. CMCC CMCC-CM2-SR5 model output prepared for CMIP6 CMIP historical. Version 20200616. *Earth System Grid Federation* **2020**. https://doi.org/10.22033/ESGF/CMIP6.3825
103. Lovato, T.; Peano, D.; Butenschön, M.; Materia, S.; Iovino, D.; Scoccimarro, E.; Fogli, P.G.; Cherchi, A.; Bellucci, A.; Gualdi, S.; Masina, S.; Navarra, S. CMIP6 simulations with the CMCC Earth System Model (CMCC1077 ESM2). *J Adv Model Earth Syst* **2022**, *14*, e2021MS002814. https://doi.org/10.1029/2021MS002814
104. Döscher, R.; Acosta, M.; Alessandri, A.; Anthoni, P.; Arneth, A.; Arsouze, T.; Bergman, T.; Bernardello, R.; Bousetta, S.; Caron, L.P.; Carver, G.; Castrillo, M.; Catalano, F.; Cvijanovic, I.; Davini, P.; Dekker, E.; Doblas-Reyes, F.J.; Docquier, D.; Echevarria, P.; Fladrich, U.; Fuentes-Franco, R.; Gröger, M.; von Hardenberg, J.; Hieronymus, J.; Karami, M.P.; Keskinen, J.P.; Koenigk, T.; Makkonen, R.; Massonet, F.; Ménégoz, M.; Miller, P.A.; Moreno-Chamarro, E.; Nieradzik, L.; van Noije, T.; Nolan, P.; O'Donnell, D.; Ollinaho, P.; van der Oord, G.; Ortega, P.; Prims, O.T.; Ramos, A.; Reerink, T.; Rousset, C.; Ruprich-Robert, Y.; Le Sager, P.; Schmith, T.; Schrödner, R.; Serva, F.; Sicardi, V.; Madsen, M.S.; Smith, B.; Tian, T.; Tourigny, E.; Uotila, P.; Vancoppenolle, M.; Wang, S.; Wårlind, D.; Willén, U.; Wyser, K.; Yang, S.; Yepes-Arbós, X.; Zhang, Q. The EC-Earth3 Earth System Model for the Climate Model Intercomparison Project 6. *Geosci Model Dev* **2022**, *15*, 2973-3020. https://doi.org/10.5194/gmd-15-2973-2022
105. Krasting, J.P.; John, J.G.; Blanton, C.; McHugh, C.; Nikonov, S.; Radhakrishnan, A.; Rand, K.; Zadeh, N.T.; Balaji, V.; Durachta, J.; Dupuis, C.; Menzel, R.; Robinson, T.; Underwood, S.; Vahlenkamp, H.; Dunne, K.A.; Gauthier, P.P.G.; Ginoux, P.; Griffies, S.M.; Hallberg, R.; Harrison, M.; Hurlin, W.; Malyshev, S.; Naik, V.; Paulot, F.; Paynter, D.J.; Ploshay, J.; Reichl, B.G.; Schwarzkopf, D.M.; Seman, C.J.; Silvers, L.; Wyman, B.; Zeng, Y.; Adcroft, A.; Dunne, J.P.; Dussin, R.; Guo, H.; He, J.; Held, I.M.; Horowitz, L.W.; Lin, P.; Milly, P.C.D.; Shevliakova, E.; Stock, C.; Winton, M.; Wittenberg, A.T.; Xie, Y.; Zhao, M. NOAA-GFDL GFDL-ESM4 model output prepared for CMIP6 CMIP historical. Version 20190726. *Earth System Grid Federation* **2018**. https://doi.org/10.22033/ESGF/CMIP6.8597
106. Boucher, O.; Denvil, S.; Levavasseur, G.; Cozic, A.; Caubel, A.; Foujols, M.A.; Meurdesoif, Y.; Cadule, P.; Devilliers, M.; Ghattas, J.; Lebas, N.; Lurton, T.; Mellul, L.; Musat, I.; Mignot, J.; Cheruy, F. IPSL IPSL-CM6A-LR model output prepared for CMIP6 CMIP historical. Version 20180803. *Earth System Grid Federation* **2018**. https://doi.org/10.22033/ESGF/CMIP6.5195
107. Tatebe, H.; Watanabe, M. MIROC MIROC6 model output prepared for CMIP6 CMIP historical. Version 20181212. *Earth System Grid Federation* **2018**. https://doi.org/10.22033/ESGF/CMIP6.5603
108. Wieners, K.H.; Giorgetta, M.; Jungclaus, J.; Reick, C.; Esch, M.; Bittner, M.; Legutke, S.; Schupfner, M.; Wachsmann, F.; Gayler, V.; Haak, H.; de Vrese, P.; Raddatz, T.; Mauritsen, T.; von Storch, J.S.; Behrens, J.; Brovkin, V.; Claussen, M.; Crueger, T.; Fast, I.; Fiedler, S.; Hagemann, S.; Hohenegger, C.; Jahns, T.; Kloster, S.; Kinne, S.; Lasslop, G.; Kornblueh, L.; Marotzke, J.; Matei, D.; Meraner, K.; Mikolajewicz, U.; Modali, K.; Müller, W.; Nabel, J.; Notz, D.; Peters-von Gehlen, K.; Pincus, R.; Pohlmann, H.; Pongratz, J.; Rast, S.; Schmidt, H.; Schnur, R.; Schulzweida, U.; Six, K.; Stevens, B.; Voigt, A.; Roeckner, E.; MPI-M MPI-ESM1.2-LR model output prepared for CMIP6 CMIP historical. Version 20190710. *Earth System Grid Federation* **2019**. https://doi.org/10.22033/ESGF/CMIP6.6595
109. Yukimoto, S.; Koshiro, T.; Kawai, H.; Oshima, N.; Yoshida, K.; Urakawa, S.; Tsujino, H.; Deushi, M.; Tanaka, T.; Hosaka, M.; Yoshimura, H.; Shindo, E.; Mizuta, R.; Ishii, M.; Obata, A.; Adachi, Y. MRI MRI-ESM2.0 model output prepared for CMIP6 CMIP historical. Version 20190222. *Earth System Grid Federation* **2019**. https://doi.org/10.22033/ESGF/CMIP6.6842
110. Chen, M.; Shi, W.; Xie, P.; Silva, V.B.S.; Kousky, V.E.; Higgins, R.W.; Janowiak, J.E. Assessing objective techniques for gauge-based analyses of global daily precipitation. *J. Geophys. Res.* **2008**, *113*, D04110. https://doi.org/10.1029/2007JD009132
111. Silva, V.C.B.; Kousky, V.E.; Shi, W.; Higgins, W. An improved gridded historical daily precipitation analysis for Brazil. *J Hydrometeorol* **2007**, *8*, 847-861. https://doi.org/10.1175/JHM598.1
112. Lee, T.; Singh, V.P. *Statistical downscaling for hydrological and environmental applications*. 1st ed.; Taylor & Francis Group: Boca Raton, Florida, United States of America, 2019.

113. Mukherjee, S.; Aadhar, S.; Stone, D.; Mishra, V. Increase in extreme precipitation events under anthropogenic warming in India. *Weather Clim Extremes* **2018**, *20*, 45-53. https://doi.org/10.1016/j.wace.2018.03.005
114. Lee, M.-H.; Lu, M.; Im, E.-S.; Bae. D.-H. Added value of dynamical downscaling for hydrological projections in the Chungju Basin, Korea. *Int J Climatol* **2019**, *39*, 516-531. https://doi.org/10.1002/joc.5825
115. Mishra, V.; Bhatia, U.; Tiwari, A.D. Bias-corrected climate projections for South Asia from Coupled Model Intercomparison Project-6. *Sci Data* **2020**, *7*, 338. https://doi.org/10.1038/s41597-020-00681-1
116. Xu, Z.; Han, Y.; Tam, C.-Y.; Yang, Z.-L.; Fu, C. Bias-corrected CMIP6 global dataset for dynamical downscaling of the historical and future climate (1979–2100). *Sci Data* **2021**, *8*, 293. https://doi.org/10.1038/s41597-021-01079-3
117. Tang, G.; Clark, M.P.; Papalexiou, S.M. EM-Earth: The Ensemble Meteorological dataset for planet Earth. *Bull Am Meteorol Soc* **2022**, *103*, E996-E1018. https://doi.org/10.1175/BAMS-D-21-0106.1
118. Wu, H.; Lei, H.; Lu, W.; Liu, Z. Future changes in precipitation over the upper Yangtze River basin based on bias correction spatial downscaling of models from CMIP6. *Environ Res Commun* **2022**, *4*, 045002. https://doi.org/10.1088/2515-7620/ac620e
119. Admasu, L.M.; Grant, L.; Thiery, W. Exploring global climate model downscaling based on tile-level output. *J Appl Meteorol Climatol* **2023**, *62*, 171-190. https://doi.org/10.1175/JAMC-D-21-0265.1
120. Tram-Anh, Q.; Ngo-Duc, T.; Espagne, E.; Trinh-Tuan, L. A 10-km CMIP6 downscaled dataset of temperature and precipitation for historical and future Vietnam climate. *Sci Data* **2023**, *10*, 257. https://doi.org/10.1038/s41597-023-02159-2
121. Logan, T.; Aoun, A.; Bourgault, P.; Huard, D.; Lavoie, J.; Rondeau-Genesse, G.; Smith, J.T.; Alegre, R.; Barnes, C.; Biner, S.; Caron, D.; Ehbrecht, C.; Fyke, J.; Keel, T.; Labonté, M.-P.; Lierhammer, L.; Low, J.-F.; Quinn, J.; Roy, P.; Whelan, C. Ouranosinc/xclim: v0.37.0 (v0.37.0). *Zenodo* **2022**. https://doi.org/10.5281/zenodo.6671565
122. Wilks, D.S. *Statistical methods in the Atmospheric Sciences*, 4th ed.; Elsevier: Cambridge, United States of America, 2019.
123. Almazroui, M.; Ashfaq, M.; Islam, M.N.; Kamil, S.; Abid, M.A.; O'Brien, E.; Ismail, M.; Reboita, M.S.; Sörensson, A.A.; Arias, P.A.; Alves, L.M.; Tippett, M.K.; Saeed, S.; Haarsma, R.; Doblas-Reyes, F.J.; Saeed, F.; Kucharski, F.; Nadeem, I.; Silva-Vidal, Y.; Rivera, J.A.; Ehsan, M.A.; Martínez-Castro, D.; Muñoz, A.G.; Ali, M.A.; Coppola, E.; Sylla, M.B. Assessment of CMIP6 performance and projected temperature and precipitation changes over South America. *Earth Syst Environ* **2021**, *5*, 155-183. https://doi.org/10.1007/s41748-021-00233-6
124. Arias, P.A.; Ortega, G.; Villegas, L.D.; Martínez, J. Colombian climatology in CMIP5/CMIP6 models: Persistent biases and improvements. Rev Fac Ing 2021, 100, 75-96. https://doi.org/10.17533/udea.redin.20210525
125. Ortega, G.; Arias, P.A.; Villegas, J.C.; Marquet, P.A.; Nobre, P. Present-day and future climate over Central and South America according to CMIP5/CMIP6 models. *Int J Climatol* **2021**, *41*, 6713–6735. https://doi.org/10.1002/joc.7221
126. Huang, F.; Xu, Z.; Guo, W. The linkage between CMIP5 climate models' abilities to simulate precipitation and vector winds. *Clim Dyn* **2020**, *54*, 4953-4970. https://doi.org/10.1007/s00382-020-05259-6
127. Torres, R.R.; Marengo, J.A. Uncertainty assessments of climate change projections over South America. *Theor Appl Climatol* **2013**, *112*, 253-272. https://doi.org/10.1007/s00704-012-0718-7
128. Rivera, J.A.; Arnould. G. Evaluation of the ability of CMIP6 models to simulate precipitation over Southwestern South America: Climatic features and long-term trends (1901-2014). *Atmos Res* **2020**, *241*, 104953. https://doi.org/10.1016/j.atmosres.2020.104953
129. Barreiro, M.; Chang, P.; Saravanan, R. Simulated precipitation response to SST forcing and potential predictability in the region of the South Atlantic Convergence Zone. *Clim Dyn* **2005**, *24*, 105-114. https://doi.org/10.1007/s00382-004-0487-9
130. Bombardi, R.J.; Trenary, L.; Pegion, K.; Cash, B.; DelSole, T.; Kinter, J.L. Seasonal predictability of summer rainfall over South America. *J Clim* **2018**, *31*, 8181-8195. https://doi.org/10.1175/JCLI-D-18-0191.1
131. Torres, R.R.; Benassi, R.B.; Martins, F.B.; Lapola, D.M. Projected impacts of 1.5 and 2 °C global warming on temperature and precipitation patterns in South America. *Int J Climatol* **2021**, *42*, 1597-1611. https://doi.org/10.1002/joc.7322
132. Ruffato-Ferreira, V.; Barreto, R.C.; Júnior, A.O.; Silva, W.L.; Viana, D.B.; Nascimento, J.A.S.; Freitas, M.A.V. A foundation for the strategic long-term planning of the renewable energy sector in Brazil: Hydroelectricity and wind energy in the face of climate change scenarios. *Renew Sustain Energy Rev* **2017**, *72*, 1124-1137. https://doi.org/10.1016/j.rser.2016.10.020
133. de Jong, P.; Barreto, T.B.; Tanajura, C.A.S.; Oliveira-Esquerre, K.P.; Kiperstok, A.; Torres, E.A. The impact of regional climate change on hydroelectric resources in South America. *Renew Energy* **2021**, *173*, 76-91. https://doi.org/10.1016/j.renene.2021.03.077

134. Medeiros, F.J.; Oliveira, C.P.; Avila-Diaz, A. Evaluation of extreme precipitation climate indices and their projected changes for Brazil: From CMIP3 to CMIP6. *Weather Clim Extrem* **2022**, *38*, 100511. https://doi.org/10.1016/j.wace.2022.100511
135. Cai, W.; McPhaden, M.J.; Grimm; A.M.; Rodrigues, R.R.; Taschetto, A.S.; Garreaud, R.D.; Dewitte, B.; Poveda, G.; Ham, Y.-G.; Santoso, A.; Ng, B.; Anderson, W.; Wang, G.; Geng, T.; Jo, H.-S.; Marengo, J.A.; Alves, L.M.; Osman, M.; Li, S.; Wu, L.; Karamperidou, C.; Takahashi, K.; Vera, C. Climate impacts of the El Niño-Southern Oscillation on South America. *Nat Rev Earth Environ* **2020**, *1*, 215-231. https://doi.org/10.1038/s43017-020-0040-3
136. Reboita, M.S.; Ambrizzi, T.; Crespo, N.M.; Dutra, L.M.M.; Ferreira, G.W.S.; Rehbein, A.; Drumond, A.; da Rocha, R.P.; Souza, C.A. Impacts of teleconnection patterns on South America climate. *Ann NY Acad Sci* **2021**, *1504*, 116-153. https://doi.org/10.1111/nyas.14592
137. Jimenez, J.C.; Libonati, R.; Peres, L.F. Drought over Amazonia in 2005, 2010, and 2015: A cloud cover perspective. *Front Earth Sci* **2018**, *6*, 227. https://doi.org/10.3389/feart.2018.00227
138. Li, J.; Huo, R.; Chen, H.; Zhao, Y.; Zhao, T. Comparative assessment and future prediction using CMIP6 and CMIP5 for annual precipitation and extreme precipitation simulation. *Front Earth Sci* **2021**, *9*. https://doi.org/10.3389/feart.2021.687976
139. Medeiros, F.J.; Oliveira, C.P. Assessment of dry and heavy rainfall days and their projected changes over Northeast Brazil in Coupled Model Intercomparison Project Phase 6 models. *Int J Climatol* **2022**, *42*, 8665-8686. https://doi.org/10.1002/joc.7759
140. Costa, M.S.; Oliveira-Júnior, J.F.; Santos, P.J.; Filho, W.L.F.C.; Gois, G.; Blanco, C.J.C.; Teodoro, P.E.; Silva Junior, C.A.; Santiago, D.B.; Souza, E.O.; Jardim, A.M.R.F. Rainfall extremes and drought in Northeast Brazil and its relationship with El Niño–Southern Oscillation. *Int J Climatol* **2020**, E2111-E2135. https://doi.org/10.1002/joc.6835
141. Cavalcanti, I.F.A. The influence of extratropical Atlantic Ocean region on wet and dry years in North-Northeastern Brazil. *Front Earth Sci* **2015**, *3*, 34. https://doi.org/10.3389/fenvs.2015.00034
142. Ruiz-Vásquez, M.; Arias, P.A.; Martínez, J.A.; Espinoza, J.C. Effects of Amazon basin deforestation on regional atmospheric circulation and water vapor transport towards tropical South America. *Clim Dyn* **2020**, *54*, 4169-4189. https://doi.org/10.1007/s00382-020-05223-4
143. Arias, P.A.; Rivera, J.A.; Sörensson, A.A.; Zachariah, M.; Barnes, C.; Philip, S.; Kew, S.; Vautard, R.; Koren, G.; Pinto, I.; Vahlberg, M.; Singh, R.; Raju, E.; Li, S.; Yang, W.; Vecchi, G.A.; Otto, F.E.L. Vulnerability and high temperatures exacerbate impacts of ongoing drought in Central South America. *World Weather Attribution* **2023**. Available at: https://www.worldweatherattribution.org/wp-content/uploads/WWA-Argentina-Uruguay-drought-Scientific-Report.pdf
144. Rivera, J.A.; Otta, S.; Lauro, C.; Zazulie, N. A decade of hydrological drought in central-western Argentina. *Front Water* **2021**, *3*. https://doi.org/10.3389/frwa.2021.640544
145. Xu, F.; Bento, V.A.; Qu, Y.; Wang, Q. Projections of global drought and their climate drivers using CMIP6 global climate models. *Water* **2023**, *15*, 2272. https://doi.org/10.3390/w15122272